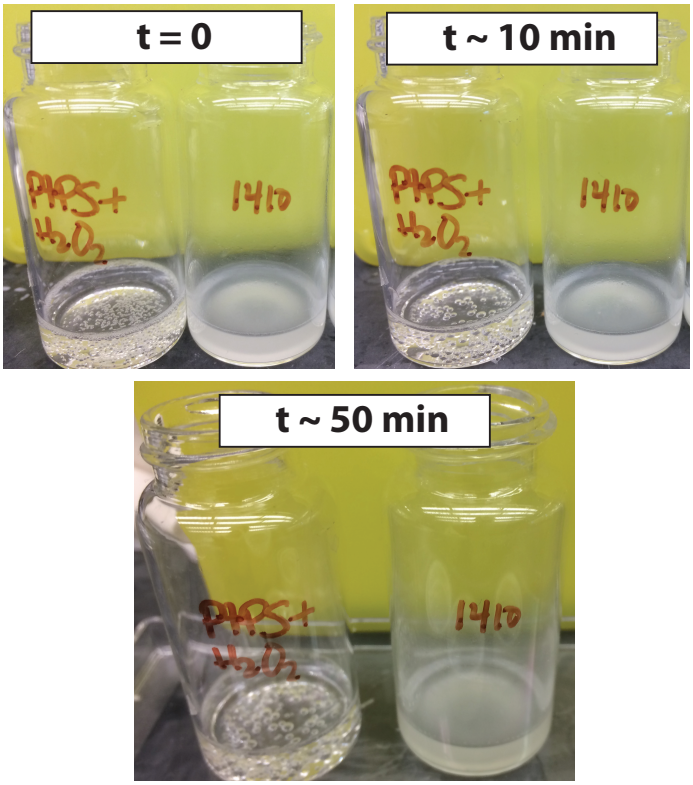

Figure 3S-5. Anti-foam chemicals for O_2 suppression. Each vial contains Platinum coated polystyrene particles with 10% H_2O_2. We compare the growth of O_2 bubbles over time with and without anti-foam chemical (Xiameter 1410, Dow Chemical). Addition of 1410 helps suppress formation of O_2 bubbles when compared to control sample without 1410.

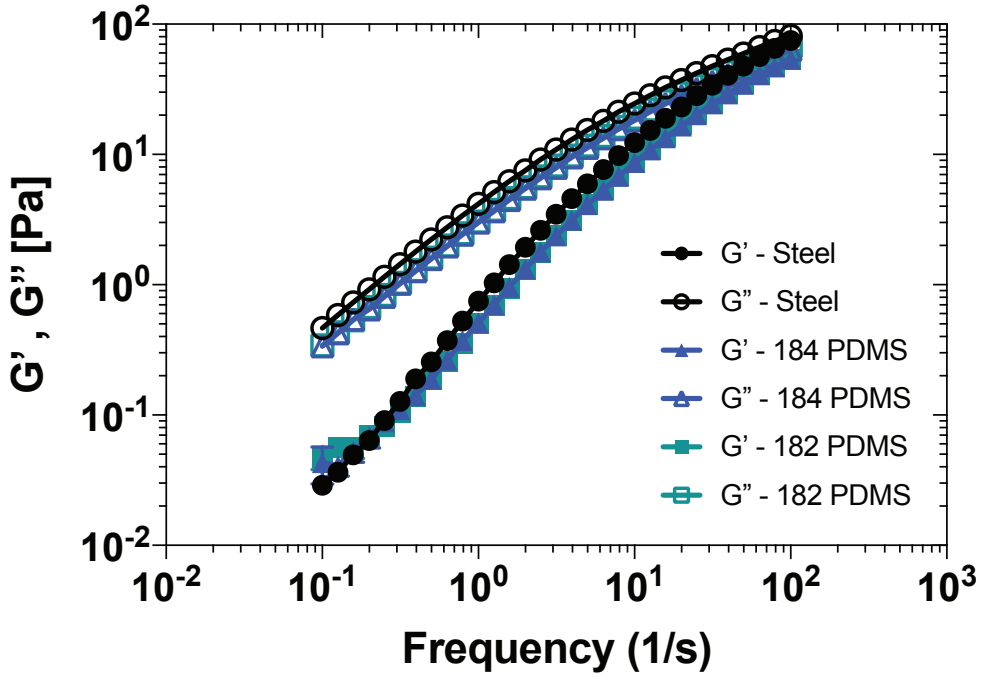

Figure 3S-6. Accuracy of steel plates with PDMS attached. Frequency sweep of 4 wt.% PEO in water solutions using stainless steel fixtures and PDMS modified fixtures. We compared the stainless steel fixtures to two different types of PDMS (Dow Sylgard 182 & Dow Sylgard 184). We find no significant difference between the traditional stainless steel fixtures and the PDMS modified fixture.

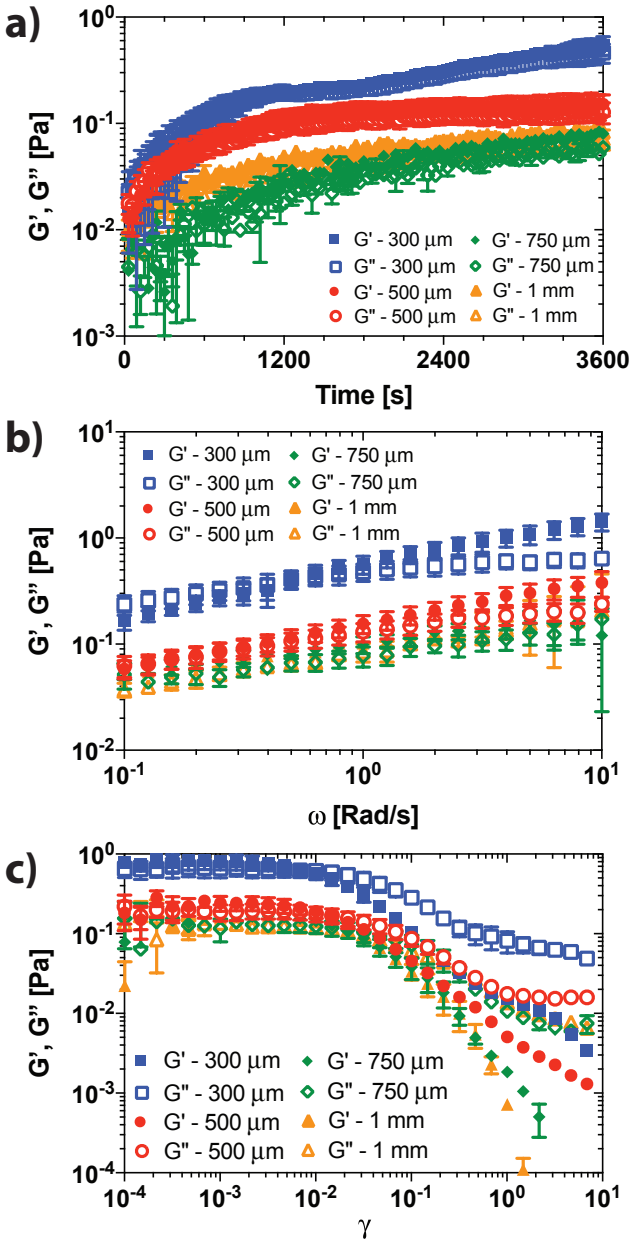

Figure 3S-7. Gap study with 50 mm steel plate. a) Time sweep was done at a frequency of 1 s^{-1} and strain of 0.003. b) Frequency sweep was performed at a fixed strain of 0.003. c) Strain sweep was done at a fixed frequency of 1 s^{-1}.

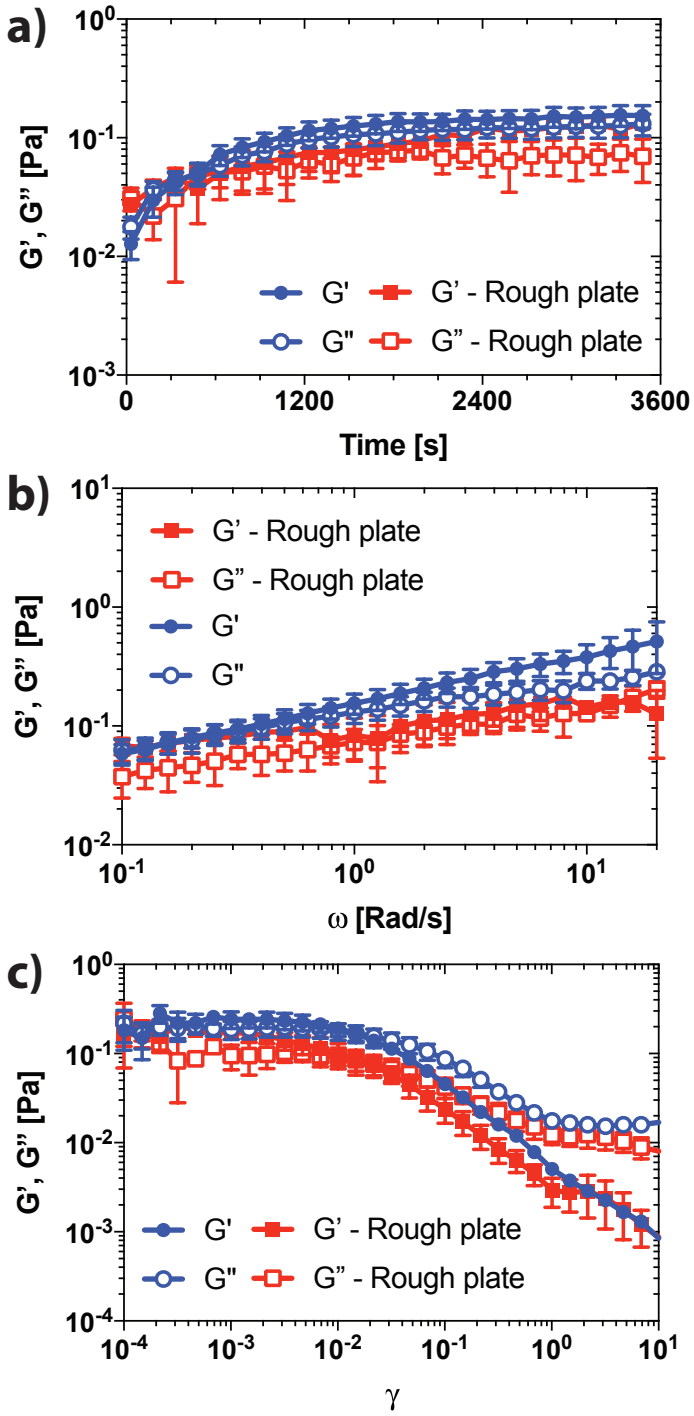

Figure 3S-8. Comparison of rheology of passive gels with steel plate and sandblasted steel plate. a) Time sweep was done at a frequency of 1 s^{-1} and strain of 0.003. b) Frequency sweep was performed at a fixed strain of 0.003. c) Strain sweep was done at a fixed frequency of 1 s^{-1}.

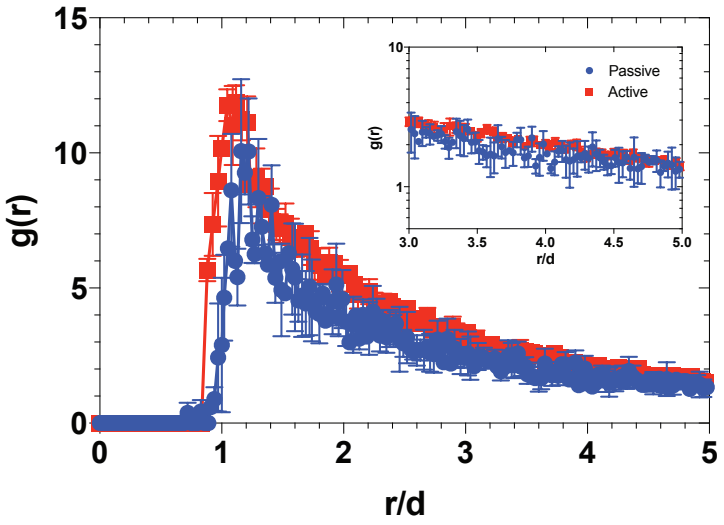

Figure 3S-9. Radial distribution function, g(r), of passive and active gels. The fractal dimension, d_f, and average cluster size, R_c, were calculated from g(r) for passive and active gels.

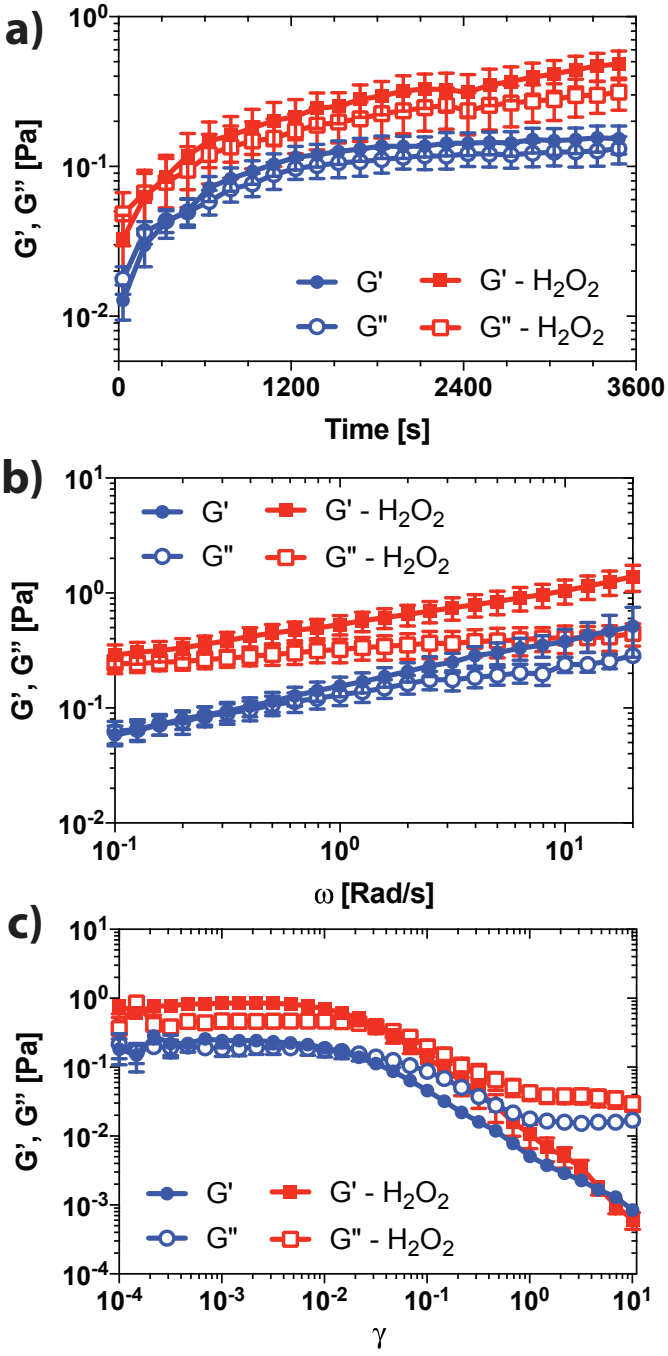

Figure 3S-10. Comparison of rheology of passive gels with and without hydrogen peroxide measured with a 50 mm steel plate. All measurements were collected at a gap of 0.5 mm at 20°C. a) Time sweep was done at a frequency of 1 rad/s and strain of 0.003. b) Frequency sweep was performed at a fixed strain of 0.003. c) Strain sweep was done at a fixed frequency of 1 rad/s. The elastic modulus of gels are stiffened by about 37.5% after addition of hydrogen peroxide.

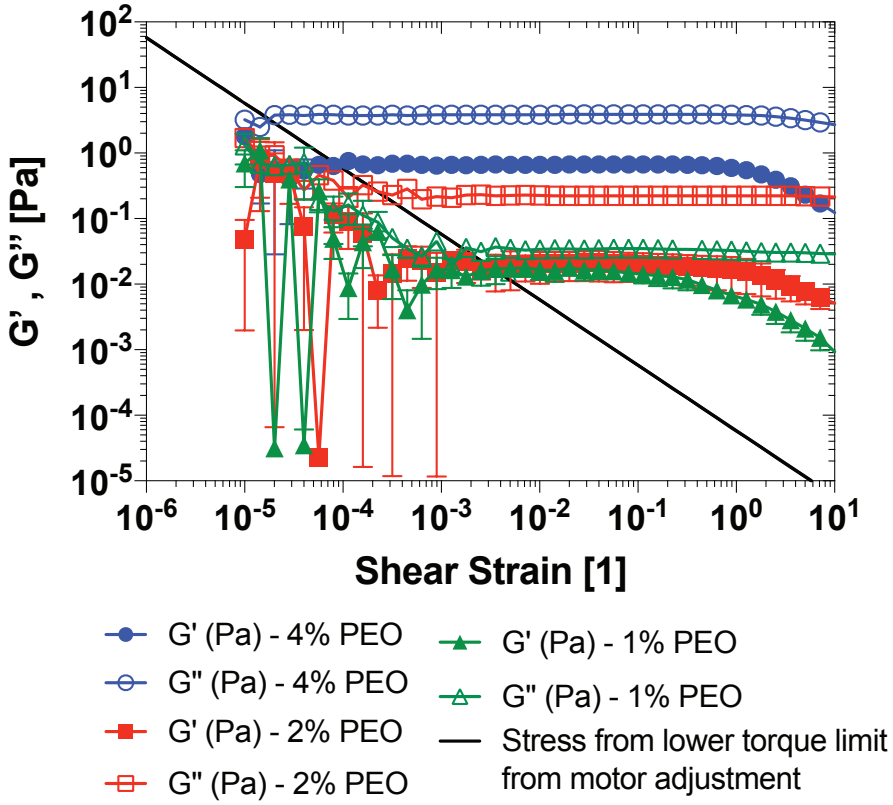

Figure 3S-11. Determining lower stress limit of the rheometer. Lower stress limit was determined from measured lower torque limit (shown in solid black line). A strain amplitude of $\gamma = 0.003$, which corresponds to an elastic modulus of 0.02 Pa.

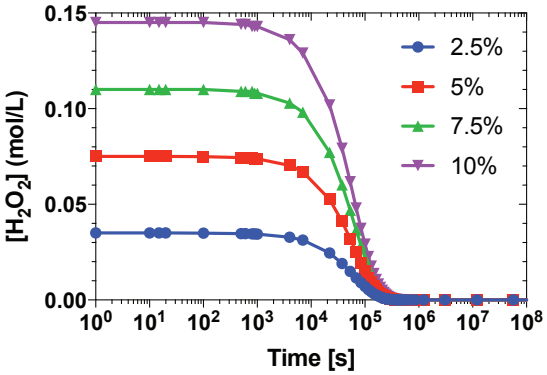

Rate Constant	Time [s]
$1 \times 10^{14}[s^{-1}\mu m^{-2}]$	10^5
$3.2 \times 10^{13}[s^{-1}\mu m^{-2}]$	10^6
$0.3 \times 10^{-4}[s^{-1}]$ (12 cm² Platinum)	10^3

Figure 3-S12. Hydrogen peroxide decomposition reaction kinetics. Left) Hydrogen peroxide concentration as a function of time determined from rate constant in Howse et. al. [6]. Right) Table shows a comparison of rate constants from literature with predicted timescales for hydrogen peroxide depletion [6, 37, 38].

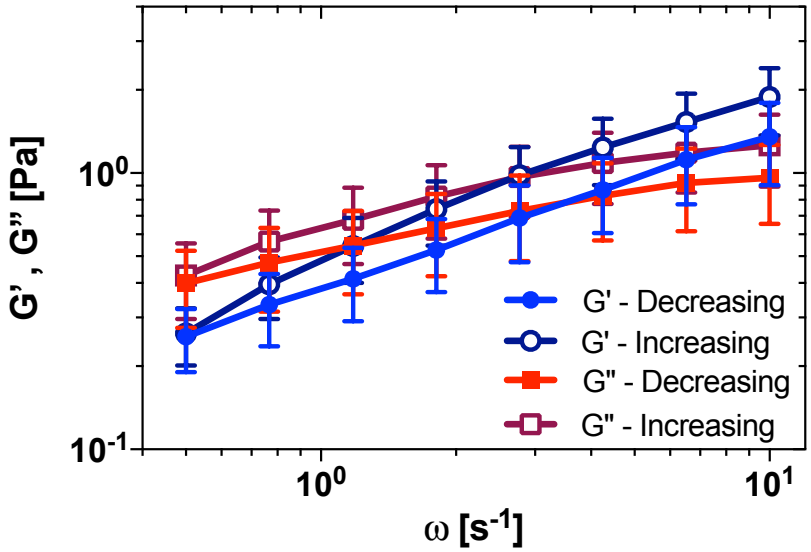

Figure 3S-13. Hysteresis during passive gel frequency sweeps. Frequency sweeps were performed 15 minutes after addition of salt from high to low frequency (which takes ~4 minutes) followed by another frequency sweep from low to high frequency.

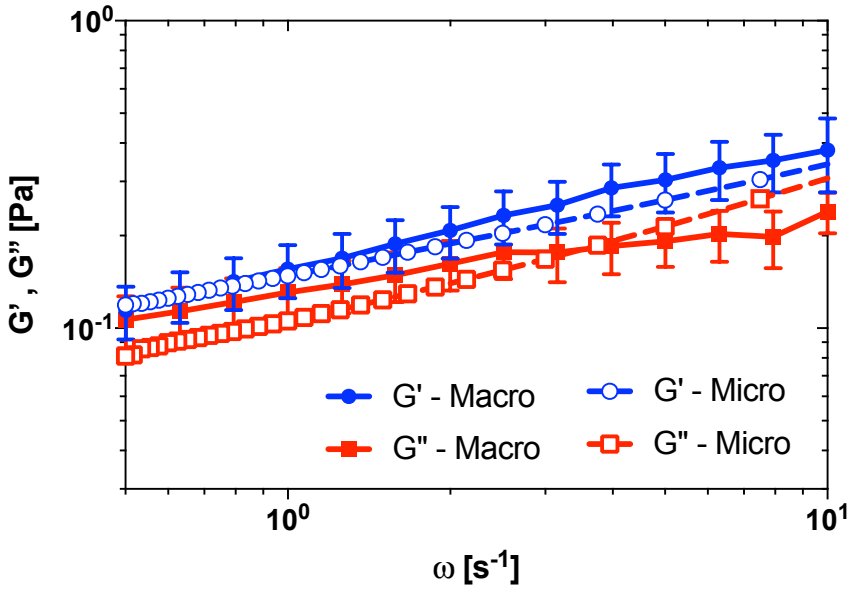

Figure 3S-14. Comparison of the viscoelastic moduli from microrheology and mechanical rheology for gels at quasi-steady state, 60 minutes after addition of salt to induce gelation.

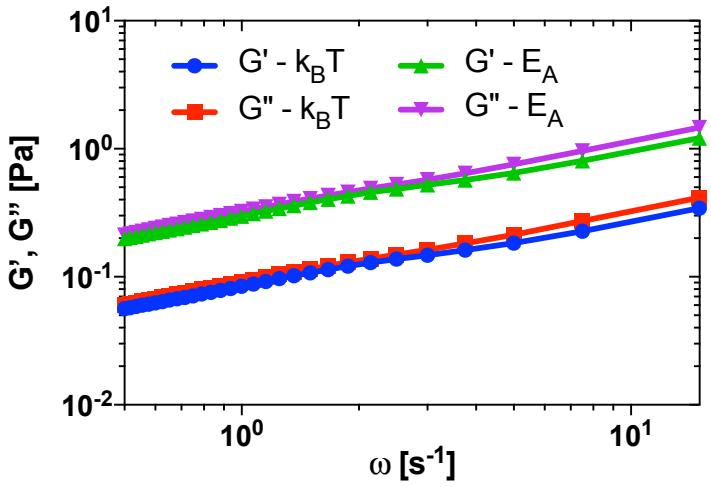

Figure 3-S15. Substituting the active energy in place of the thermal energy in the generalized Stokes-Einstein equation for microrheology. Use of the active energy yields an even higher prediction of the frequency dependent viscoelastic moduli of active gels.

3.8 References

[1] B. M. Mognetti, a. Šarić, S. Angioletti-Uberti, a. Cacciuto, C. Valeriani, and D. Frenkel, Phys. Rev. Lett. **111**, 1 (2013).

[2] J. Palacci, S. Sacanna, A. P. Steinberg, D. J. Pine, and P. M. Chaikin, Science. **339**, 936 (2013).

[3] E. J. Hemingway, A. Maitra, S. Banerjee, M. C. Marchetti, S. Ramaswamy, S. M. Fielding, and M. E. Cates, Phys. Rev. Lett. **114**, 1 (2015).

[4] S. J. Ebbens and J. R. Howse, Soft Matter **6**, 726 (2010).

[5] S. Sánchez, L. Soler, and J. Katuri, Angew. Chemie Int. Ed. **54**, 1414 (2015).

[6] J. R. Howse, R. A. L. Jones, A. J. Ryan, T. Gough, R. Vafabakhsh, and R. Golestanian, Phys. Rev. Lett. **99**, 048102 (2007).

[7] W. F. Paxton, S. Sundararajan, T. E. Mallouk, and A. Sen, Angew. Chemie - Int. Ed. **45**, 5420 (2006).

[8] N. H. P. Nguyen, D. Klotsa, M. Engel, and S. C. Glotzer, Phys. Rev. Lett. **112**, 075701 (2014).

[9] S. McCandlish, A. Baskaran, and M. Hagan, Soft Matter **8**, 2527 (2012).

[10] B. van der Meer, L. Filion, and M. Dijkstra, **12**, 3406 (2016).

[11] D. Mizuno, C. Tardin, C. F. Schmidt, and F. C. MacKintosh, Science. **315**, 370 (2007).

[12] T. B. Liverpool, M. C. Marchetti, J.-F. Joanny, and J. Prost, Europhys. Lett. **85**, 18007 (2009).

[13] H. M. López, J. Gachelin, C. Douarche, H. Auradou, and E. Clément, Phys. Rev. Lett. **115**, 1 (2015).

[14] D. T. N. Chen, A. W. C. Lau, L. A. Hough, M. F. Islam, M. Goulian, T. C. Lubensky, and A. G. Yodh, Phys. Rev. Lett. **99**, 1 (2007).

[15] V. Prasad, V. Trappe, A. D. Dinsmore, P. N. Segre, L. Cipelletti, and D. A. Weitz, Faraday Discuss. **123**, 1 (2003).

[16] E. Zaccarelli, J. Phys. Condens. Matter **19**, 323101 (2007).

[17] L. C. Hsiao, R. S. Newman, S. C. Glotzer, and M. J. Solomon, Proc. Natl. Acad. Sci. **109**, 16029 (2012).

[18] W.-H. Shih, W. Y. Shih, S.-I. Kim, J. Liu, and I. A. Aksay, Phys. Rev. A **42**, 4772 (1990).

[19] R. Mezzenga, P. Schurtenberger, A. Burbidge, and M. Michel, Nat. Mater. **4**, 729 (2005).

[20] M. H. Lee and E. M. Furst, Phys. Rev. E **77**, 041408 (2008).

[21] A. H. Krall and D. A. Weitz, Phys. Rev. Lett. **80**, 778 (1998).

[22] M. Lattuada, H. Wu, and M. Morbidelli, Chem. Eng. Sci. **59**, 4401 (2004).

[23] M. E. Szakasits, W. Zhang, and M. J. Solomon, Phys. Rev. Lett. **119**, (2017).

[24] W. B. Russel, D. A. Saville, and W. R. Schowalter, *Colloidal Dispersions* (Cambridge University Press, 1989).

[25] A. A. Shah, B. Schultz, K. L. Kohlstedt, S. C. Glotzer, and M. J. Solomon, Langmuir **29**, 4688 (2013).

[26] Z. Németh, G. Rácz, and K. Koczo, J. Colloid Interface Sci. **207**, 386 (1998).

[27] A. J. O'Lenick, J. Surfactants Deterg. **3**, 229 (2000).

[28] S. C. Takatori, W. Yan, and J. F. Brady, Phys. Rev. Lett. **113**, 028103 (2014).

[29] D. Allan, L. Uieda, F. Boulogne, R. W. Perry, T. A. Caswell, and N. Keim, (2014).

[30] J. Crocker and D. Grier, J. Colloid Interface Sci. **310**, 298 (1996).

[31] L. C. Hsiao, B. A. Schultz, J. Glaser, M. Engel, M. E. Szakasits, S. C. Glotzer, and M. J. Solomon, Nat. Commun. **6**, 8507 (2015).

[32] T. Savin and P. S. Doyle, Biophys. J. **88**, 623 (2005).

[33] D. Dendukuri, D. C. Pregibon, J. Collins, T. A. Hatton, and P. S. Doyle, Nat. Mater. **5**, 365 (2006).

[34] B. R. Dasgupta, S.-Y. Tee, J. C. Crocker, B. J. Frisken, and D. A. Weitz, Phys. Rev. E **65**, 051505 (2002).

[35] M. Carpineti and M. Giglio, Phys. Rev. Lett. **68**, 3327 (1992).

[36] L. Cipelletti, S. Manley, R. C. Ball, and D. A. Weitz, Phys. Rev. Lett. **84**, 2275 (2000).

[37] D. W. McKee, J. Catal. **14**, 355 (1969).

[38] M. A. Hasnat, M. M. Rahman, S. M. Borhanuddin, A. Siddiqua, N. M. Bahadur, and M. R. Karim, Catal. Commun. **12**, 286 (2010).

[39] S. Mazoyer, L. Cipelletti, and L. Ramos, Phys. Rev. Lett. **97**, 8 (2006).

[40] S. C. Takatori and J. F. Brady, Soft Matter **10**, 9433 (2014).

[41] D. Z. Rocklin, L. C. Hsiao, M. Szakasits, M. J. Solomon, and X. Mao, ArXiv Soft Condens. Matter 1 (2018).

Chapter 4 Hydration kinetics and rheology of psyllium polysaccharide gels

4.1 Abstract

Psyllium is a polysaccharide extracted from plant seeds and is commonly used as a dietary fiber supplement. Upon mixing with water, psyllium powders swell to form a gel phase. Under some conditions, the gel undergoes syneresis, resulting in a gel phase enriched in psyllium underneath a polymer-poor aqueous phase. In this work, we investigate the transition from powder to gel for three different commercially available psyllium grades with varying physical characteristics, including grain size. The purpose of this work is to understand the role of hydration kinetics on gel stability and macroscopic rheology of psyllium suspensions. We measure the steady-state rheology of the three psyllium materials as a function of concentration and find there are few differences among the linear viscoelastic moduli, G' and G", as well as the shear-rate dependent viscosity of the gels. However, transient rheological measurements collected during gelation show significant differences in the gelation kinetics of the three different psyllium materials; gels prepared from psyllium powders with the smallest grain size exhibited a low viscosity at short times. To further investigate the role of gelation kinetics, we characterize the microdynamics of the material's hydration. By using a fluorescent dye that binds with the psyllium grains, we visualized the hydration-induced expansion the psyllium powders at concentrations as large as 97%. Characteristic hydration times extracted from the measurements vary from 30 s to 60 s among the three

powders; hydration times decay with increasing powder concentration by a factor of 5 for the fine and 9 for the medium powder. Hydration time increases by a factor of 2 with increasing concentration of coarse powder. We find gel stability is higher in psyllium materials that have a high viscosity at short times.

4.2 Introduction

Polysaccharides are naturally occurring polymers that are abundant in plants and animals [1]. Their chemical structure varies, but always includes glycoses, or monosaccharides, that are covalently bonded by an O-glycosidic bond [2]. The degree of polymerization for polysaccharides is typically greater than 100 and as large as several hundred thousand, resulting in a high molecular weight polymer [2]. Their molar mass is therefore typically in the range of 10^6 Da [3]. The thickening and gelling properties of polysaccharides make them useful in a variety of industries such as food, cosmetics, and biomedical applications [4]. Polysaccharides exhibit non-Newtonian rheological behavior, such as shear banding [5], thixotropy [6], shear thinning [4], or thermal induced thickening [7]. Broadly, polysaccharides are common gelators because of the large quantity of free hydroxyl groups that can form hydrogen bonds with water [3].

Less work has examined the kinetic processes of hydration and gelation of polysaccharides. Understanding the relationship between hydration and gelation time and their effects on transient rheology can aid in the design of materials in the multiple industries in which polysaccharides are used, especially for applications in which hydration kinetics is important to their value. (Three examples of such applications are the formulation of polysaccharides to control the water retention of cement mixtures, [8] the incorporation of polysaccharides into wound dressings, [9] and the time required for

gels to set in foods that use polysaccharides as gelators. [10]) Furthermore, characterizing the transition from powder to gel in these materials can contribute towards an understanding of the physics of gelation and syneresis in complex polymer systems.

Here we study the hydration-induced transition from powder to gel of psyllium fiber, derived from the plant *Plantago ovata*. Psyllium is a hemi-cellulosic seed mucilage and is most frequently used as a dietary fiber supplement [11,12]. Upon mixing with water, psyllium powders absorb liquid, and the material expands to form a gel. The ability of psyllium fiber to uptake water makes it useful for a number of applications including: synthesizing renewable hydrogels [13]; improving the binding properties of cement or concrete [14]; and, increasing stability and bioavailability in pharmaceutical formulations [15]. The chemical structure of psyllium is comprised of a xylan backbone with xylose and arabinose side chains, resulting in a comb-like polymer structure [12]. The side chains can be modified to alter the structure, swelling, and rheological properties of psyllium [12,16]. Psyllium husk is extracted from the seeds, which can then be ground into a powder. The powder grains have a primarily amorphous structure [17]. The typical psyllium grain size is 100 – 425 μm [18,19].

Previous rheological studies of psyllium gels have focused on characterizing equilibrium gels as a function of concentration, temperature, or pH [20]. In these materials, the elastic modulus (G') is larger than the viscous modulus (G") at concentrations as low as 2.0 wt%, indicating that the sample is solid-like even at these low concentrations. Temperature sweeps have shown a phase transition around 40°C, where there is a rapid increase in the modulus as temperature increased followed by a plateau in G' and G" at temperatures higher than 40°C, which was described as

correlating with re-arrangement of inter or intra molecular hydrogen bonds [20]. To our knowledge, no work has examined the transient structure, dynamics, and rheology of psyllium fiber as it undergoes hydration and gelation.

In this work, we characterize the kinetics of psyllium fiber expansion as it undergoes hydration and gelation from both macroscopic and microscopic perspectives. We study three different commercially available psyllium samples that differ in their average gain size. We observe that gels prepared from psyllium with the smallest grain size are more prone to syneresis than the other two. We characterize the rheology of the psyllium gels over the concentration range, 0.5% - 10 wt. %. Through measurements of the gel samples across several concentrations, we find that there is little difference in the steady-state values of the shear-rate dependent viscosity and the frequency dependent linear viscoelastic moduli G', and G". However, by means of transient oscillatory and viscosity measurements, we find that the three different psyllium materials differ in their gelation kinetics. Specifically, the gel that undergoes syneresis has a much lower transient viscosity than at steady-state. The stable gels attain steady-state viscosity much more rapidly than the gel undergoing syneresis. We further characterize the hydration kinetics by imaging psyllium powder contact with water (i.e. hydration) with confocal microscopy. We find the rate of hydration decreases with increasing concentration with the fine and medium psyllium powders; while we observe a slight increase in the rate of hydration with increasing concentration of the coarse powder. Our results have implications for the design of materials made from hydrating polysaccharides; specifically, it highlights the relevance of transient viscous properties to gel syneresis.

4. 3 Materials and methods

Preparation of psyllium gels

Three types of commercially available psyllium fiber with varying powder size were used for measurements: fine, medium, and coarse powder (Metamucil, Now Foods Powder, and Now Foods Husk). Gels for syneresis measurements were prepared by weighing desired amount of psyllium and HPLC water (purchased from Sigma Aldrich) followed by vigorous vortex mixing for about 30 seconds. Samples were rolled overnight before measurement. Gels for transient measurements were prepared by weighing psyllium to a glass vial, adding water, and shaking the vial to quickly mix the solution.

Gel stability studies

Gel stability studies were performed by adding the desired amount of psyllium material to a 4 mL glass vial. We add HPLC water (purchased from Sigma Aldrich) to the vial and quickly shake to mix the psyllium and water. Gel syneresis was analyzed approximately 5 minutes after mixing, with the images of Figure 1 taken at that time.

Rheological characterization

Steady-state measurements of the linear viscoelastic properties of psyllium gels were measured with a rheometer (ARG2, TA instruments) equipped with a parallel plate geometry (60 mm stainless steel). A solvent trap was used to minimize effects of evaporation. A gap study was performed for the psyllium powders at 2.5%, SI Figure 1. The gap study showed G' and G" insensitive to gap dimension for gaps larger than 750 μm for the medium powder and 1.5 mm for the coarse powder; consequently, the gap used for gels prepared with fine and medium powder was 1.0 mm. For the coarse

powder, a gap of 2.0 mm was used. Small amplitude oscillatory shear measurements were performed with a strain amplitude of $\gamma = 0.01$ and a frequency of $\omega = 0.1$ Hz. All measurements were performed at T = 25°C.

We check for slip in the transient measurements by comparing the viscoelastic moduli and viscosity for 2.5 wt. % fine powder with a smooth and sandblasted steel fixture, Figure S2. We observe a modest difference in the transient measurements between the smooth and sandblasted fixtures; however, there are no significant effects of slip. Transient viscosity measurements were collected with a sandblasted steel fixture at a fixed strain rate of $\dot{\gamma} = 0.003$ s^{-1}.

Visualization of hydration and microscopic dynamics

Single and multi-grain hydration of the fine and medium psyllium powders was imaged using a confocal laser-scanning microscope (CLSM; Nikon A1Rsi Confocal Microscope, NA = 0.3, 10x objective). Coarse powder multi-grain hydration was imaged using a 4x objective, NA = 0.13. To prepare samples for imaging, UV glue (Loctite 3301) was spread onto a clean glass slide and psyllium grains were deposited onto it; subsequent exposure to UV light confined the grains to the slide. Fluorescent stain (Calcofluor white, purchased from Sigma-Aldrich) was used to image the grains as they underwent hydration. This stain is useful because it binds with the outer mucilage layer of psyllium during hydration and fluoresces upon exposure to UV light [12,21]. The emission maximum of this dye is 433 nm for an excitation frequency of 355 nm. We add 25 uL of the fluorescent dye to the fine and medium psyllium powders and 75 uL of dye to the coarse powder and vary the amount of psyllium deposited onto the slides. We scan a 512 x 512 pixel image with a pixel size of 2.49 μm/pixel and record a 5-minute video at

a frame rate of 0.47 fps. To process images, CLSM data is converted to binary images using image thresholding algorithms in Fiji [22,23]. We use the complex hull algorithm in Sci-Kit image to convert the binary images from single grain hydration experiments to an area fraction. The area fraction for multi grain hydration was characterized using total number of pixels from the binary images. The time-dependence of the area fraction quantifies the rate of expansion for single and multi grain hydration of the psyllium powders. [22,24]

4.4 Results

Gelation, gel stability, and syneresis

We prepare psyllium gels using three different types of psyllium – fine, medium, and coarse powder. To characterize the gel stability of the materials, samples were prepared at 2.5 and 5.0 wt.% psyllium in water. (These concentrations were chosen because they approximate recommended dosages of psyllium in dietary applications.) Figure 1 shows the gel stability of each psyllium sample at a) 2.5% and b) 5.0%. The medium and coarse psyllium powder form a homogenous gel phase at 2.5%; however, the fine powder undergoes rapid syneresis into a gel phase under a clarified aqueous phase. (An analysis of N = 5 samples at 2.5% indicated that the fine powder gels always undergoes syneresis, the medium powder formed a uniform gel 4 out of 5 times, and the coarse psyllium always formed a uniform gel.) The gel boundary in each sample is marked in Figure 1. On the other hand, all three gels prepared at 5.0% form a more homogenous gel phase. Images of gels in Figure 1 were taken ~ 5 minutes after sample preparation.

The presence of the partition boundary in the gels prepared with fine powder at 2.5% concentration suggests there may be differences in gel cohesiveness and stability among the psyllium materials. Specifically, physical processes governing the formation of a stable gel are sedimentation, dynamical arrest, and attractive bonding. The psyllium grains have a higher density than water ($\rho_{H_2O} = 1.0$ g/mL and $\rho_{psyllium} = 1.35$ g/mL [25]). Sedimentation could therefore trigger the consolidation and syneresis of hydrated grains. Physical processes curbing the propensity to sediment are dynamical arrest, which would lock the grains in a glassy, vitrified structure or attractive bonding which would trap the grains in a sample-spanning network [26]. A specific aim of this work is to understand why one specimen is prone to sedimentation at a certain concentration, whereas the other two are not, as well as correlate that observation with other measurable physical properties of the materials.

Steady-state and transient rheology of psyllium gels

Steady state rheological measurements were performed on each of the psyllium samples through small amplitude oscillatory shear at variable frequency and fixed strain amplitude of 0.01. Figure 2 shows the linear elastic and storage moduli, G' and G", respectively, as a function of frequency for the three psyllium samples over the concentration range of 0.5 – 5.0 wt. %. Figure 2 shows G' is always greater than G" across the full range of frequencies, indicating that all specimens are solid-like gels at all concentrations.

We also compared the steady-state viscosity of the gels at psyllium concentrations of 0.5%, 1.25%, 2.5%, and 5.0%, shown in Figure 3. The shear-rate dependent viscosity

indicates that the psyllium gels exhibit a plateau value of the viscosity at low shear rates and shear thinning behavior as the shear rate is increased.

Using the Cross model [27], the zero shear viscosity, η_0, was determined from the steady state flow curves in Figure 3 for each concentration.

$$\eta = \eta_\infty + \frac{\eta_o - \eta_\infty}{1 + (C\dot{\gamma})^m} \quad (1)$$

Equation 1 was used to fit data from Figure 3, where η_∞ is the infinite shear viscosity, C is related to the critical shear rate, and m is a rate constant varying between 0-1. Figure 4a shows that the zero-shear viscosity increases as a function of concentration. Consistent with the steady-state oscillatory measurements, the steady-state flow curves of the three different psyllium materials exhibit little difference.

The steady-state elastic modulus (G') and viscous modulus (G") are reported as a function of concentration at a fixed frequency, ω = 0.1 Hz, in Figure 4b. The elastic and viscous moduli both increase linearly with concentration. We observe minimal variation in the values of G' and G" among the three psyllium types in the concentration range of 0.5 – 10 wt. %.

To characterize the kinetics of gelation, transient rheological measurements were performed for the 2.5% and 5.0% psyllium samples. Small amplitude oscillatory shear flow was applied for two hours at a fixed strain amplitude, γ =0.01, and frequency, ω=0.1 Hz. Figure 5 shows G' and G" as a function of concentration at a) 2.5% and b) 5% with steady-state measurements also indicated as a dotted line. At 2.5% and 5%, the gels prepared with medium and coarse powder initially overshoot the plateau values of G' and G", but relax to a plateau value by ~10^3 seconds. G' and G" for gels prepared with 2.5% fine powder reach a plateau around 400 seconds, but the viscoelastic moduli are lower

than the medium and coarse powders. At 5%, the fine powder G' and G" increases until ~ 200 seconds, but reaches a lower plateau value than the medium and coarse powder.

Transient measurements of the viscosity were likewise performed at a fixed shear rate of 0.003 s^{-1}; this shear rate was selected because it is in the low shear plateau of the steady-state viscosity. Figure 6 shows the transient viscosity as a function of time for a) 2.5 wt.% and b) 5.0 wt.% psyllium. At both concentrations the medium and coarse powder quickly reaches the steady state viscosity (by t ~ 100 sec); whereas the fine powder increases until t ~ 500 seconds and reaches a plateau viscosity that is lower than steady state viscosity. The 5% coarse powder gel increases until ~ 200 seconds but then decreases at longer times. The decrease in viscosity could be a result of syneresis happening in the rheometer or the applied shear rate could disrupt the gel structure. At 2.5 and 5 wt. %, we observe the gel prepared from the fine powder has a lower viscosity than the other two powders; empirically, we observe the same specimen is prone to sedimentation and characterized by slow rheokinetics.

Microscopic dynamics and hydration kinetics

To characterize the hydration kinetics of the psyllium gels at the microscopic level, we observed and quantified the hydration of single grains of the three psyllium materials. We also observed hydration of multiple grains in close proximity, to gauge the role of interaction effects. We add an aqueous fluorescent dye to the dry psyllium deposited onto a coverslip and capture time series videos during hydration at the spectral emission of the dye. The dye adheres to the psyllium and fluoresces [12,21]. We observe that each of the three psyllium types expands significantly as the grains absorb water. See Figures 7, 8, and 9 for an example single grain image series for each psyllium type.

10, 11, and 12 report corresponding images for multi-grain experiments at the particular surface density of ~ 50%, which is within the range of 20% to 97% that was studied. Broadly, the grain hydration is a remarkable, dynamical process. Grains appear to swell in diameter by as much as a factor of eight. The hydration process itself is quite hierarchical, with components of the grain swelling sequentially, reminiscent of unfolding.

To analyze the hydration kinetics of the psyllium, we convert the fluorescent images videos into binary images and calculate the area of the hydrating psyllium material over time from the binary images using the ratio of on-pixels to the total number of pixels.

$$A = \frac{\#\ On\ Pixels}{Total\ \#\ Pixels} \times 100 \tag{2}$$

Single-grain hydration measurements were analyzed using two different methods: 1) using a complex hull algorithm and 2) the number of on-pixels obtained from the binary images. The complex hull algorithm fits a convex polygon using the outermost pixels of the object [24]. For each of these methods, we determine the surface coverage as a function of time. Equation 3 was used to fit the hydration data and extract a characteristic timescale for hydration:

$$A(t) - A(0) = \frac{1}{G_1}[1 - \exp(-\alpha t)] \tag{3}$$

where $A(0)$ is the initial area fraction of the psyllium grain, G_1 is determined by the final volume fraction of the hydrated grain, and α describes the rate of hydration.

Figure 7a shows the area fraction as a function of time obtained from the complex hull method. We compare values of α obtained from the complex hull algorithm to values obtained from the on-pixel abundance of the binary images, SI Figure 2. We find that

these two methods produce similar results for the fine powder ($\alpha_{CH} = 0.02 \pm 0.008$ s^{-1} and $\alpha_{WP} = 0.025 \pm 0.006$ s^{-1}, $p = 0.24$) and medium powder ($\alpha_{CH} = 0.016 \pm 0.01$ s^{-1} and $\alpha_{WP} = 0.015$ s^{-1}). The two methods show a larger, but still statistically non-significant, discrepancy for the coarse powder ($\alpha_{CH} = 0.04 \pm 0.01$ s^{-1} and $\alpha_{WP} = 0.02 \pm 0.01$ s^{-1}, $p = 0.19$). The two methods do not produce differences that are statistically significant across any of the three psyllium materials.

Single grain hydration experiments showed that fine and medium powder had comparable hydration times, $\alpha_f^{-1} = 50 \pm 14$ s and $\alpha_m^{-1} = 62.5 \pm 24$ s. The coarse psyllium powder hydrates more quickly than the fine and medium powder, $\alpha_c^{-1} = 27 \pm 12$ s. Statistical testing showed the fine and medium powder hydration times were not significantly different from each other ($p = 0.7$). Comparison of the coarse powder hydration times to the fine ($p = 0.024$) and medium ($p = 0.018$) did show a significant difference. The hydration time for the coarse powder is faster than both the fine and medium psyllium powders.

To probe the multi-grain hydration of the three types of psyllium, we confine varying amounts of psyllium to a coverslip and add the fluorescent dye, as for single grain hydration. Because it is more challenging to fit a shape to each individual grain, we quantify the area fraction versus time using just the second method: that is, the total number of on-pixels as determined from the binary images. (The relative agreement between the two methods for single grain characterization offers a degree of confidence about the fidelity of this method.)

From the multi-grain hydration experiments, we determine the rate of hydration as a function of concentration. The concentration dependence of the hydration rate

characterizes how grain crowding – the physical interaction of neighboring particles during the expansion – affects the swelling dynamics. Figure 7b shows α^{-1} as a function of concentration for the three types of psyllium. The hydration time for the fine and medium psyllium powder decreases with increasing concentration by a factor of 5 for the fine powder and 9 for the medium powder. This decrease suggests that crowding effects from neighboring grains slow down the rate of expansion of these two materials. The hydration times for coarse psyllium shows a gradual increase in the hydration time with increasing concentration by a factor of 2. However, the amount of increase for the coarse psyllium multi-grain hydration is very small, which indicates the coarse psyllium hydration time is relatively independent of concentration.

4.5 Discussion

In this work, we determined the kinetics of hydration of psyllium powder as it undergoes hydration and gelation by both microscopic and macroscopic means. The steady-state rheology of three psyllium products – fine, medium, and coarse powder – showed very little rheological variation – either in linear viscoelasticity or in the viscosity of steady-state gels. This congruence shows that at steady-state the three types of psyllium formed gels with equivalent mechanical properties. This absence of differences in steady-state rheology is noteworthy because of the difference in gel stability observed. Specifically, one of the specimens (gels prepared with fine powder) is much more prone to gel syneresis than the other two.

Interestingly, transient rheological measurements showed significant differences among the three materials. While medium and coarse powders quickly reached steady-state values, the fine powder samples took much longer to reach steady-state – requiring

more than two hours. Perhaps not coincidentally, the sample that exhibited syneresis also displayed the anomalous transient rheology. We further characterized the hydration of the psyllium gels using confocal microscopy. Multi-grain hydration experiments showed that crowding effects were more prominent in the fine and medium psyllium powder samples. The hydration time for the fine and medium powder decreased with increasing concentration; whereas, the coarse psyllium hydration time showed a slight increase with increasing concentration.

Single and multi grain hydration dynamics did not show significant differences between the fine and medium psyllium powders. Both samples have comparable single grain hydration times, and both displayed a decrease in hydration time with concentration by a factor of 5 for the fine powder and 9 for the medium powder. We observe that the hydration dynamics of the coarse psyllium are quite different than the fine and medium powders. Comparison of the single grain hydration kinetics indicates that the coarse hydration is significantly quicker than the other two, and the multi-grain experiments showed that the hydration time was relatively independent of concentration. The increase in hydration time with increasing concentration of the coarse powder is unexpected. Increasing concentration of psyllium should lead to quicker hydration times as inter-grain interactions should lead to crowding and jamming of the grains as they are expanding during hydration.

The timescales observed in microscopic hydration experiments (~60 seconds) are comparable to the time scales to reach a plateau value in the viscoelastic moduli and viscosity observed in transient rheology experiments (~100 seconds). While the medium size powder demonstrated quicker gelation kinetics during transient rheology

experiments than the fine powder, microdynamical measurements of the hydration times between the two materials were statistically indistinguishable. The coarse psyllium samples did show quicker gelation kinetics in both the transient rheology measurements and microdynamical measurements. In comparing the microdynamics with the transient rheology across all three samples, the time scales observed for gelation kinetics measured through rheology are related to the physical process of grain expansion. The differences between the values of the viscosity and viscoelastic moduli measured during transient rheology experiments suggest there are additional factors that control the gel stability and rheology of psyllium gels, such as grain size, molecular weight, or chemical interactions. Future work should look for additional origins of the transient rheology than grain unfolding. Possibilities that would warrant future study include a systematic study with varying grain size, molecular weight distribution, or investigating chemical interactions such as crystallinity or functional groups on the psyllium grains.

This study shows a correlation between gel stability and the rheokinetics. Figure 1 shows the presence of a partition boundary in gels prepared with the fine powder, which correlates with the slower gelation kinetics seen in transient rheology experiments. The medium and coarse powders demonstrated improved gel stability at 2.5%; this sample also showed fast rheokinetics. The high viscosity of materials with fast rheokinetics could slow down the effects of sedimentation in the gels. If the timescale for gelation is faster than the timescale for sedimentation, the syneresis could be retarded. However, multi-grain hydration experiments do not corroborate trends seen through transient rheology measurements.

Here, we analyzed the rheology and microdynamics of three different psyllium materials during hydration and gelation. Having found significant differences in the gelation kinetics observed through mechanical rheology between the three materials, future studies could investigate a wider range of particle sizes to probe the relationship between powder physical and chemical properties, gel stability, and gelation kinetics. The characterization results and methods used here can be used to investigate connections between gel stability, transient rheology, and hydration in a range of polysaccharide systems used in food, pharmaceutical, and consumer products applications.

4.6 Acknowledgements

We acknowledge discussion with S. Razavi during initial development of this study. This work is supported by grant NSF DMR 1408817. M. E. S. acknowledges support by a Rackham Merit Fellowship.

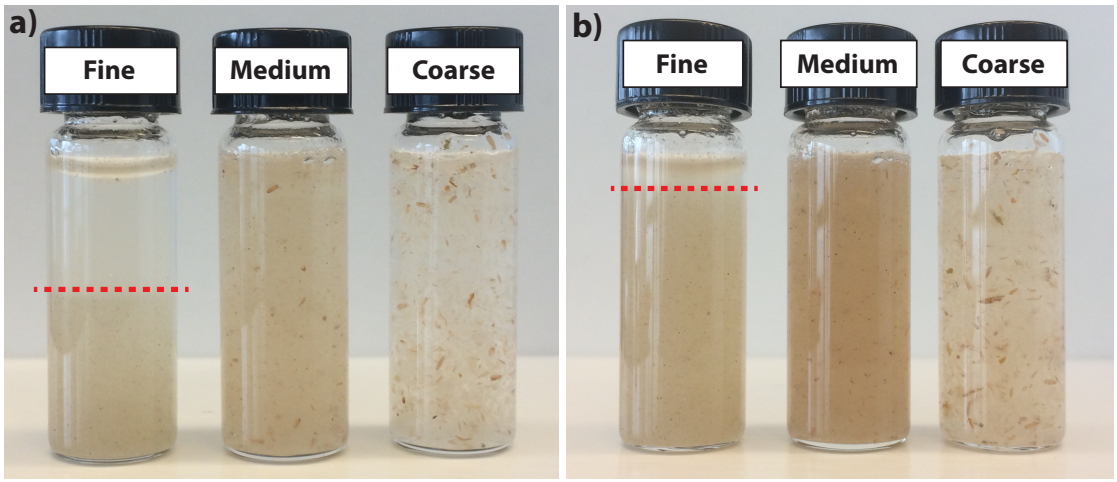

Figure 4-1. Gel stability studies of psyllium gels at a) 2.5% and b) 5% psyllium in water. The partition boundary in the gels prepared with the fine psyllium powder are indicated with a red dotted line.

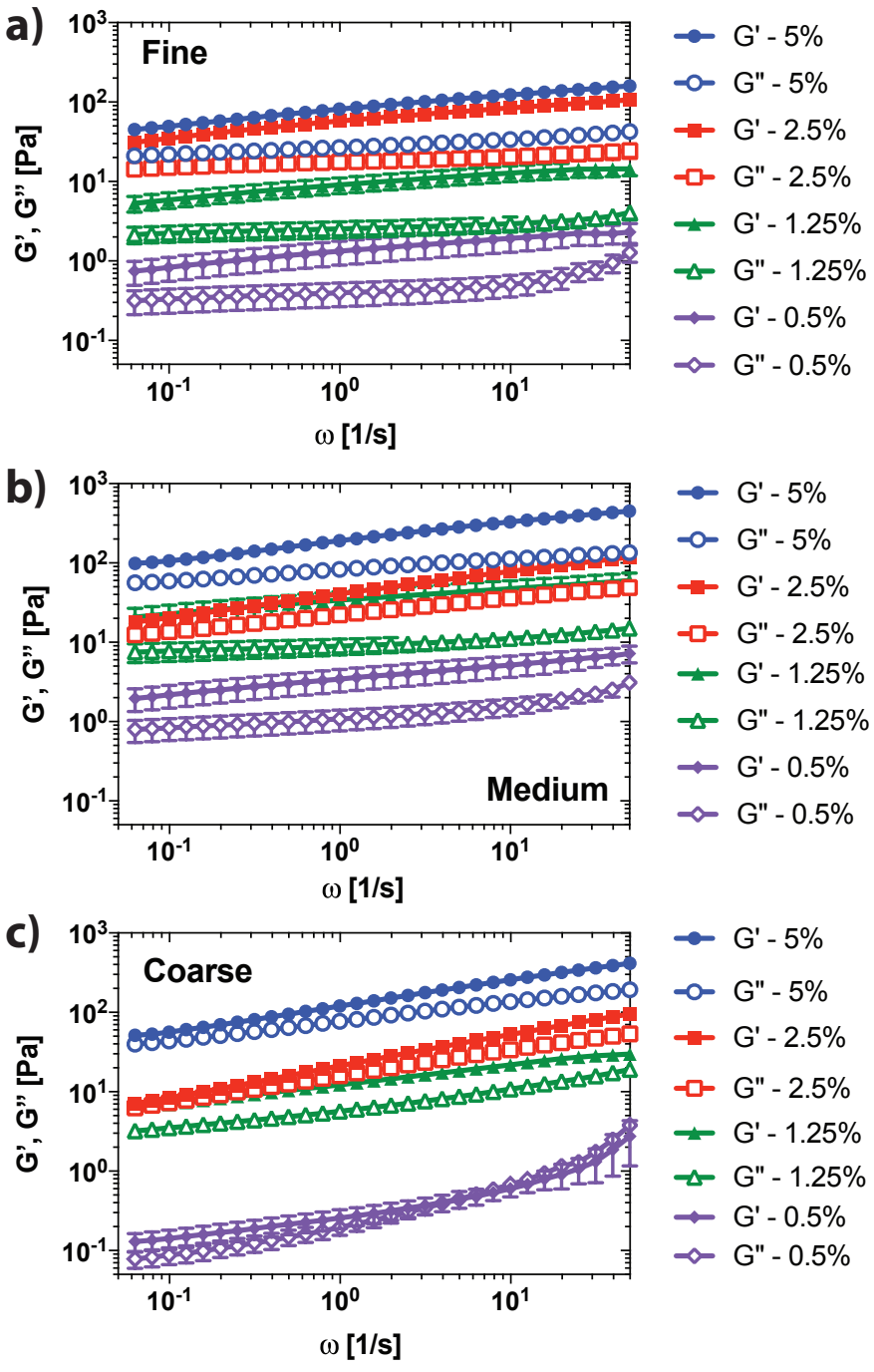

Figure 4-2. Steady state elastic (G') and viscous modulus (G") as a function of frequency (γ = 0.01) for psyllium gels prepared with a) fine, b) medium, and c) coarse psyllium powder. Closed symbols indicate G' and opened symbols are G".

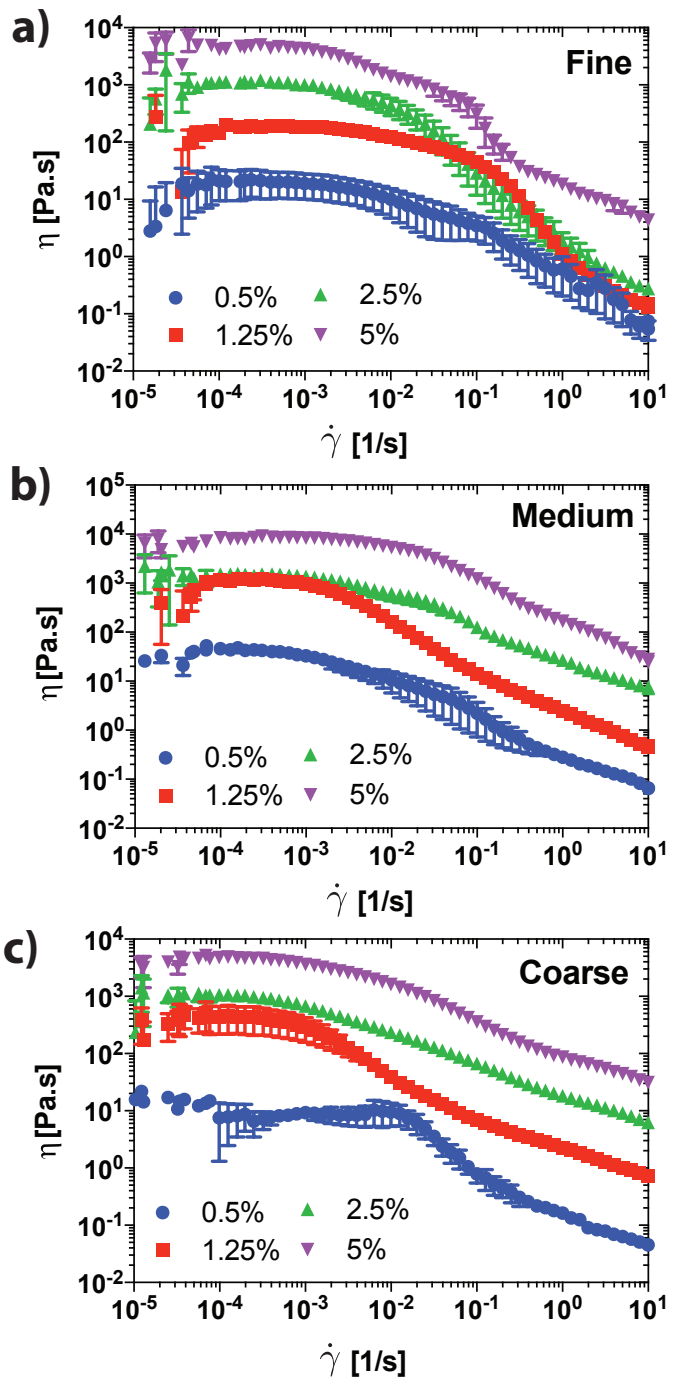

Figure 4-3. Steady state flow curves for gels prepared with a) fine, b) medium, and c) coarse psyllium powders at 0.5%, 1.25%, 2.5%, and 5%.

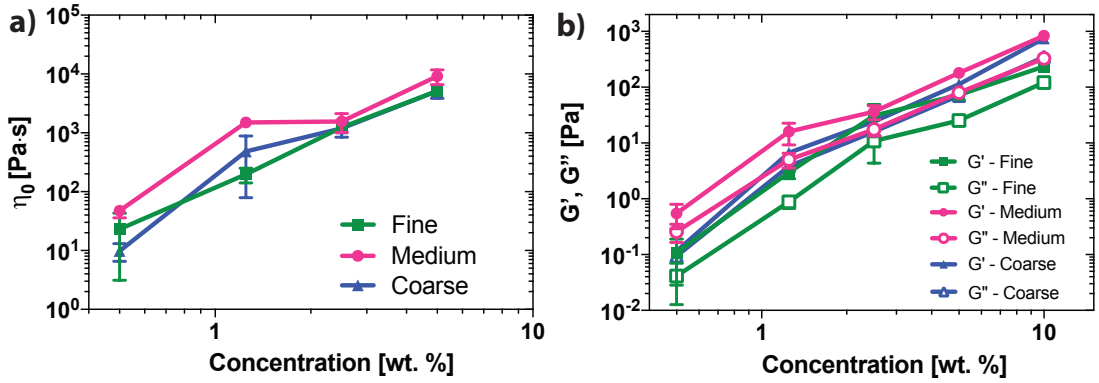

Figure 4-4. Steady state rheology of psyllium gels. a) Zero shear viscosity obtained from steady state flow curves as a function of concentration. b) Steady state elastic (G') and viscous modulus (G") as a function of concentration (γ = 0.01, ω = 0.1 Hz). Closed symbols indicate G' and opened symbols are G".

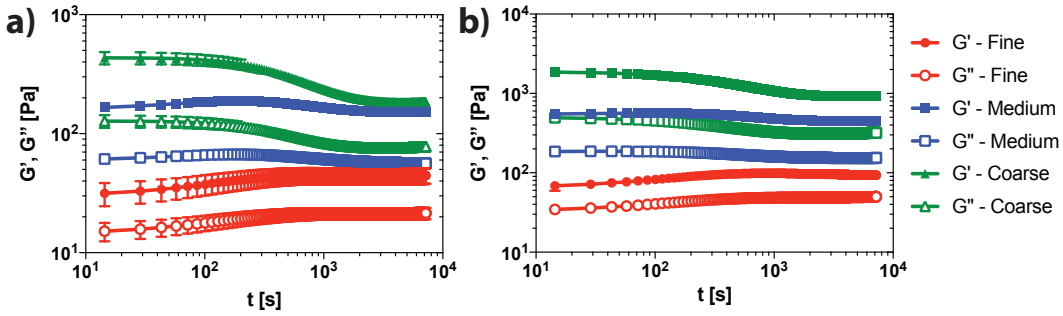

Figure 4-5. Transient oscillatory rheology of psyllium gels prepared at a) 2.5% and b) 5% ($\gamma = 0.01$, $\omega = 0.1$ Hz).

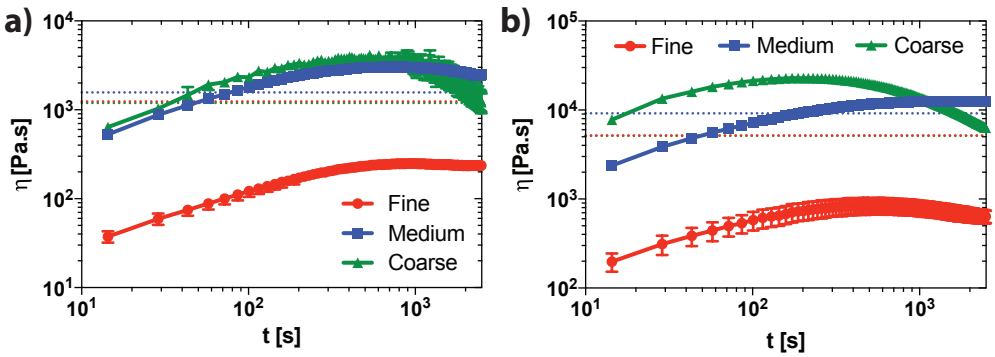

Figure 4-6. Transient viscosity of psyllium gels at a) 2.5% and b) 5% obtained at a fixed shear rate of 0.003 s^{-1}. (Steady state values shown as dotted lines).

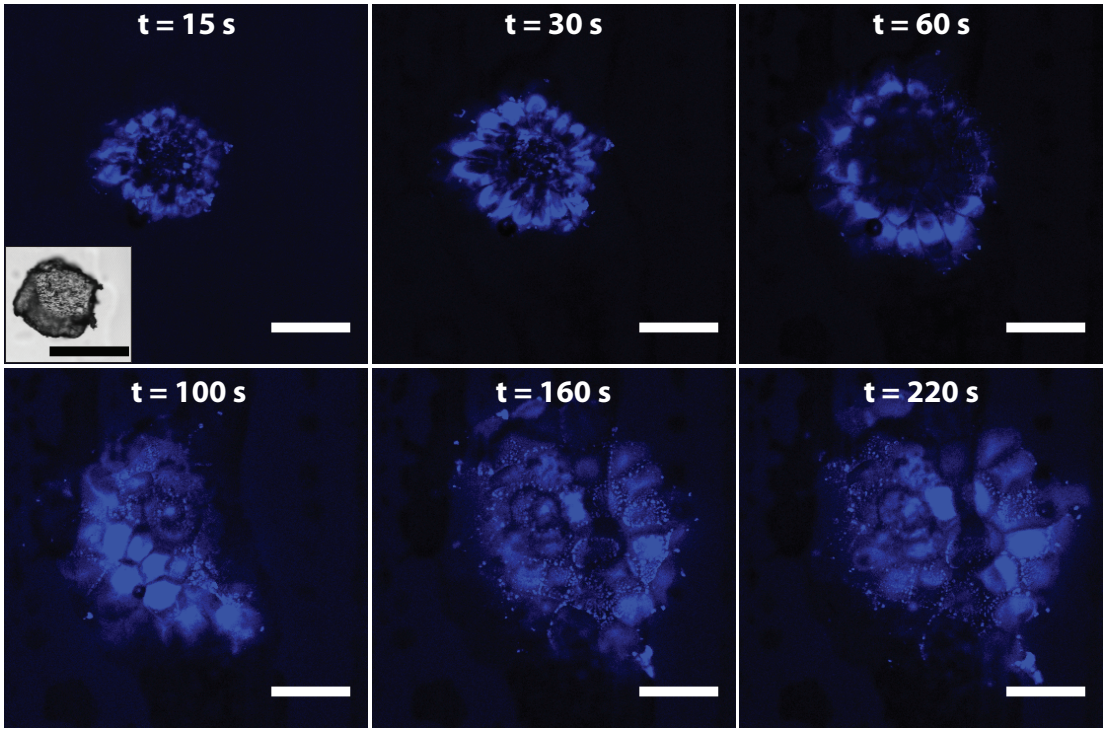

Figure 4-7. Single grain hydration of medium psyllium powder. Inset shows transmission micrograph of psyllium grain before hydration. Scale bar is 200 μm.

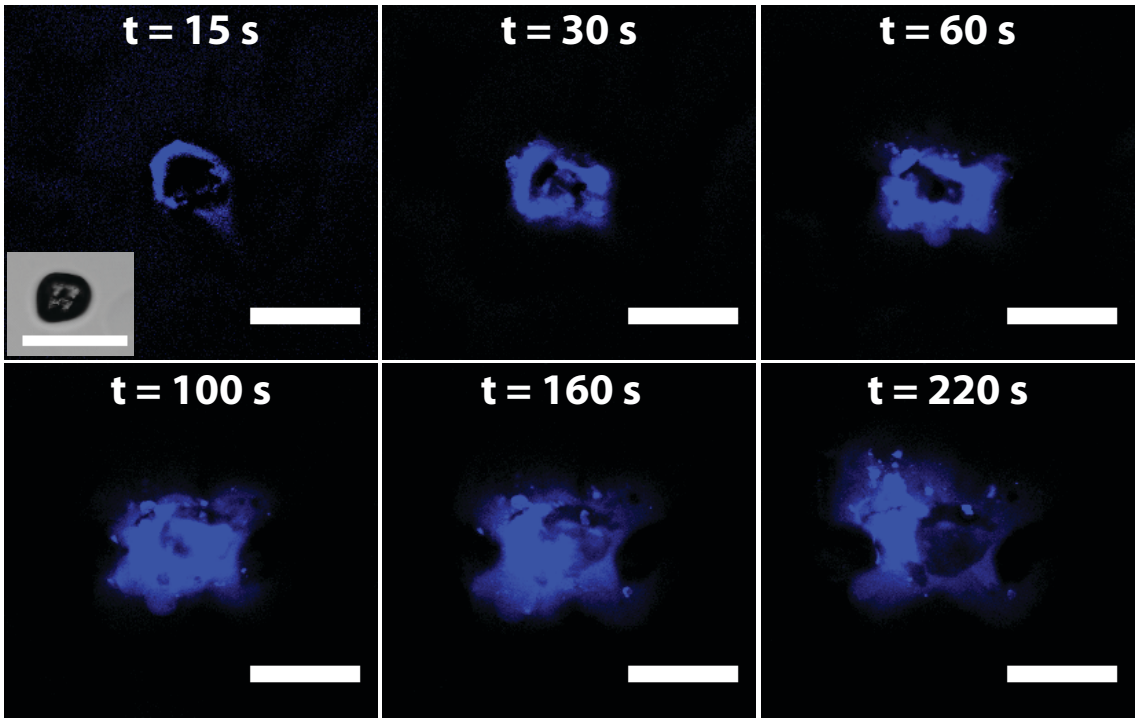

Figure 4-8. Single grain hydration of fine psyllium powder. Inset shows transmission micrograph of psyllium grain before hydration. Scale bar is 200 μm.

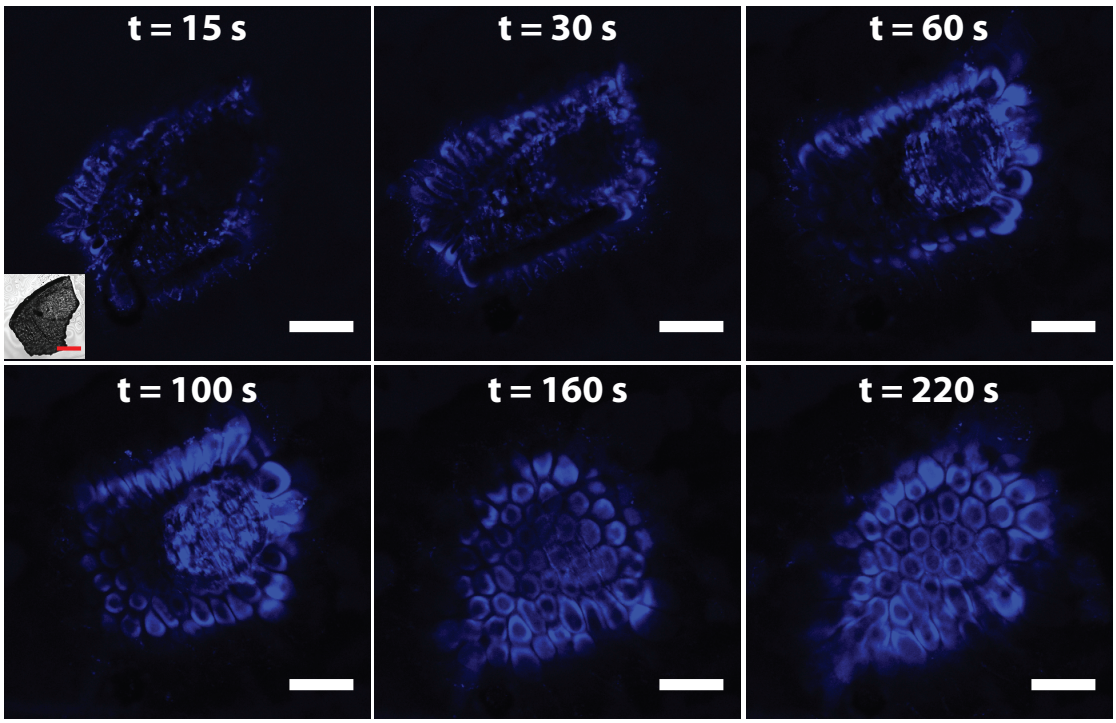

Figure 4-9. Single grain hydration of coarse psyllium powder. Inset shows transmission micrograph of psyllium husk before hydration. Scale bar is 200 μm.

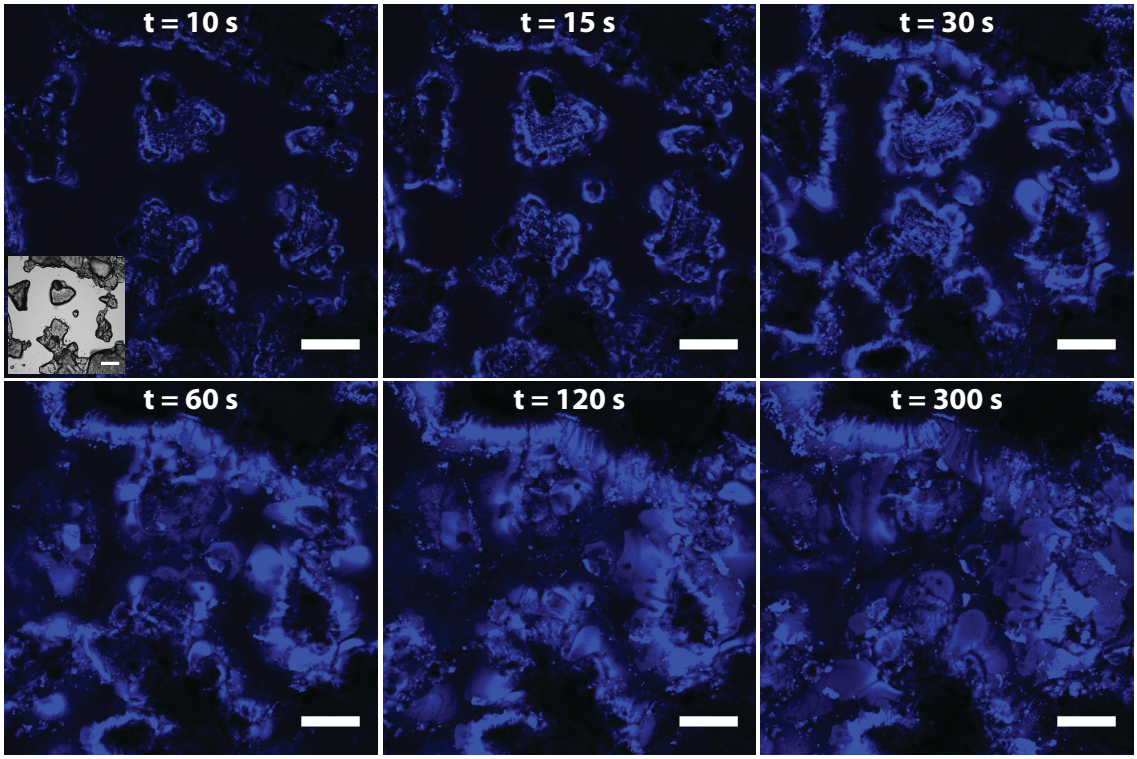

Figure 4-10. Multi-grain hydration of medium psyllium powder. Inset shows transmission micrograph of psyllium grains before hydration. Initial area of grains is ~ 50%. Scale bar is 200 μm.

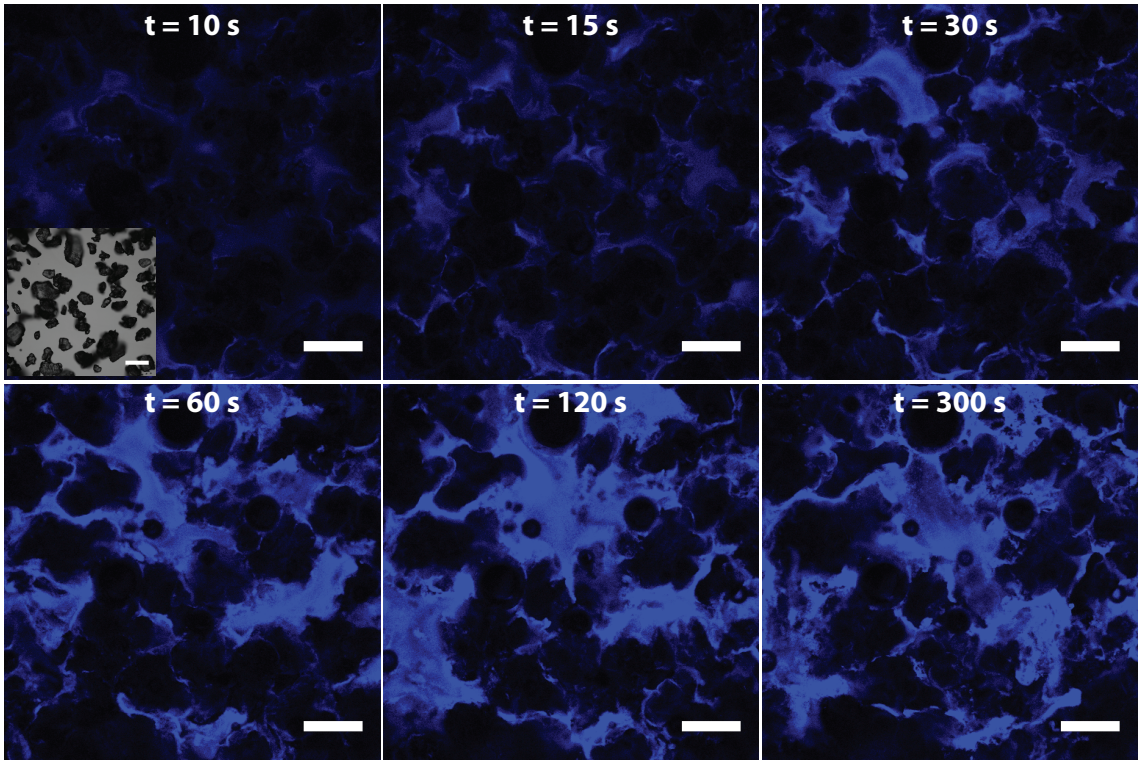

Figure 4-11. Multi-grain hydration of fine psyllium powder. Inset shows transmission micrograph of psyllium grain before hydration. Initial area of grains is ~ 50%. Scale bar is 200 μm.

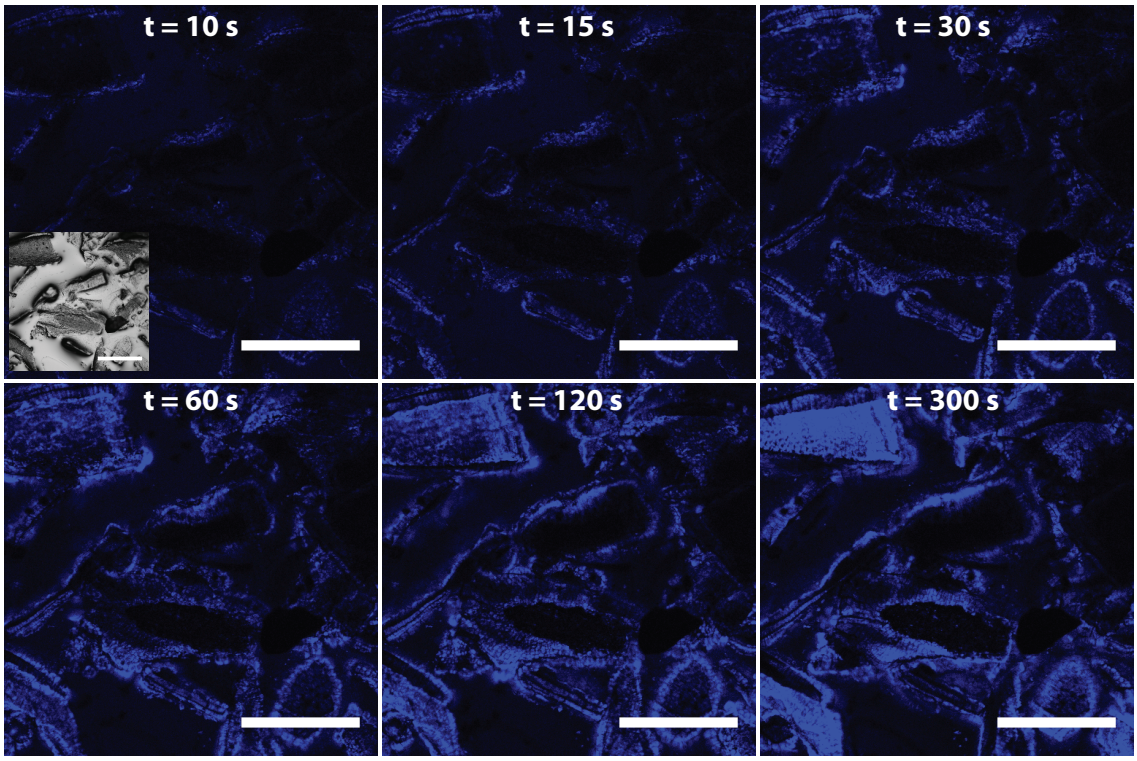

Figure 4-12. Multi-grain hydration of coarse psyllium powder. Inset shows transmission micrograph of psyllium grain before hydration. Initial concentration is ~ 50%. Scale bar is 200 μm.

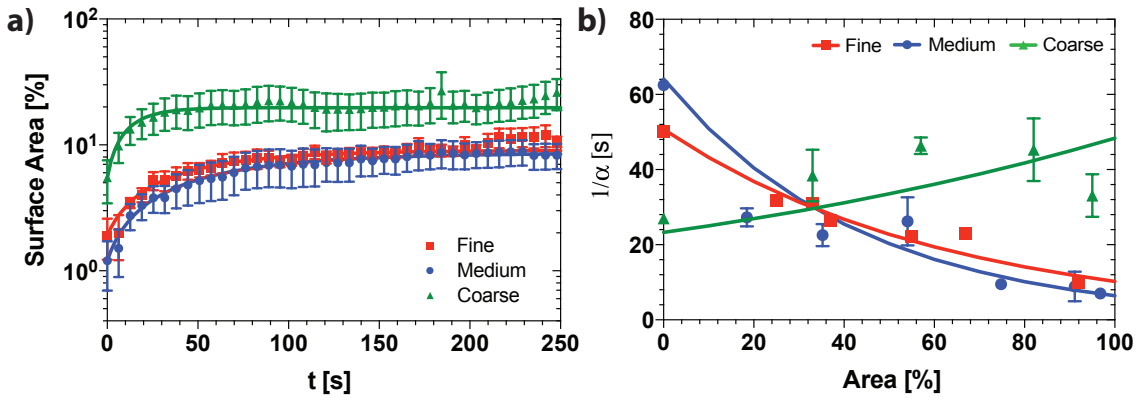

Figure 4-13. Psyllium hydration kinetics. a) Surface area as a function of time for single grain hydration. Points are experimental values and solid line is the fit from equation 3. b) Hydration time as a function of concentration from multi-grain hydration.

4.7 Supplemental Information

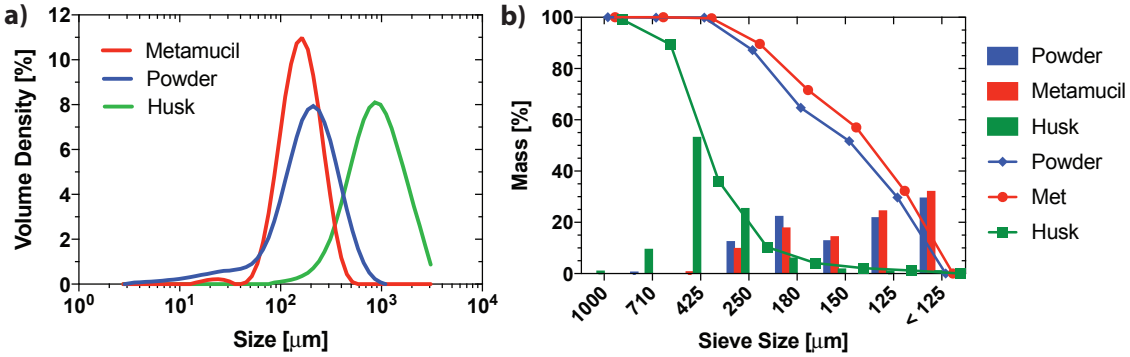

Figure 4S-1. Particle size analysis of three different psyllium materials (contributed by Particle Technology Labs). a) Laser diffraction analysis of the dry powders and b) sieve stack analysis, bars indicate mass percentage in each sieve and lines indicate cumulative percentage.

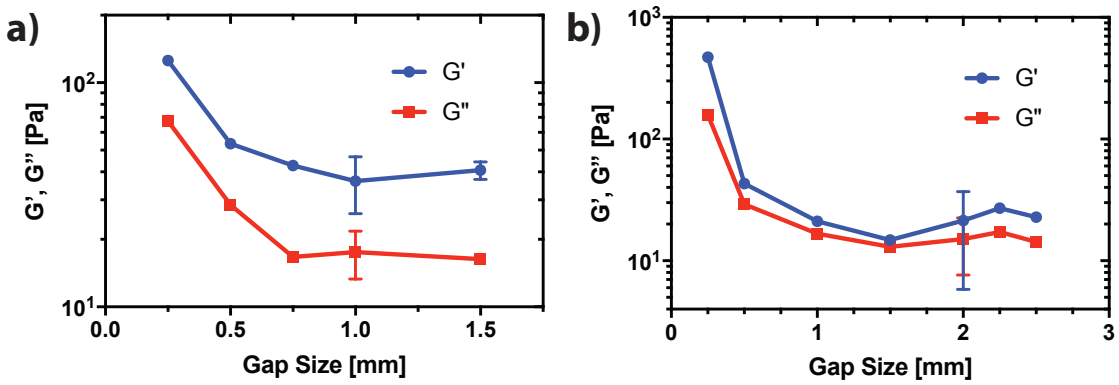

Figure 4S-2. Psyllium gel gap study. To ensure there were no gap effects for each rheological measurement, a gap study of a) medium and b) coarse powder was performed. For the medium powder, G' and G" reaches a steady value after a gap of 750 um. For the coarse psyllium, G' and G" reaches a steady value after 1.5 mm. For all rheological measurements, a gap of 1 mm was used for the fine and medium psyllium powder while 2mm was used for the coarse psyllium.

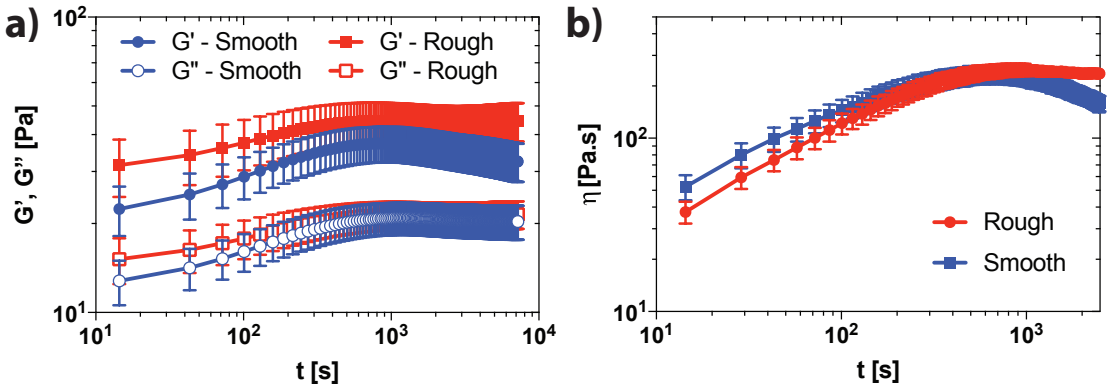

Figure 4-S3. Slip effects during transient rheology measurements. Transient oscillatory measurements for the 2.5 wt. % fine psyllium powder were collected with a smooth and roughened parallel plate. Measurements of the transient a) viscoelastic moduli and b) viscosity show a modest difference in the viscoelastic moduli and viscosity with the roughened fixtures.

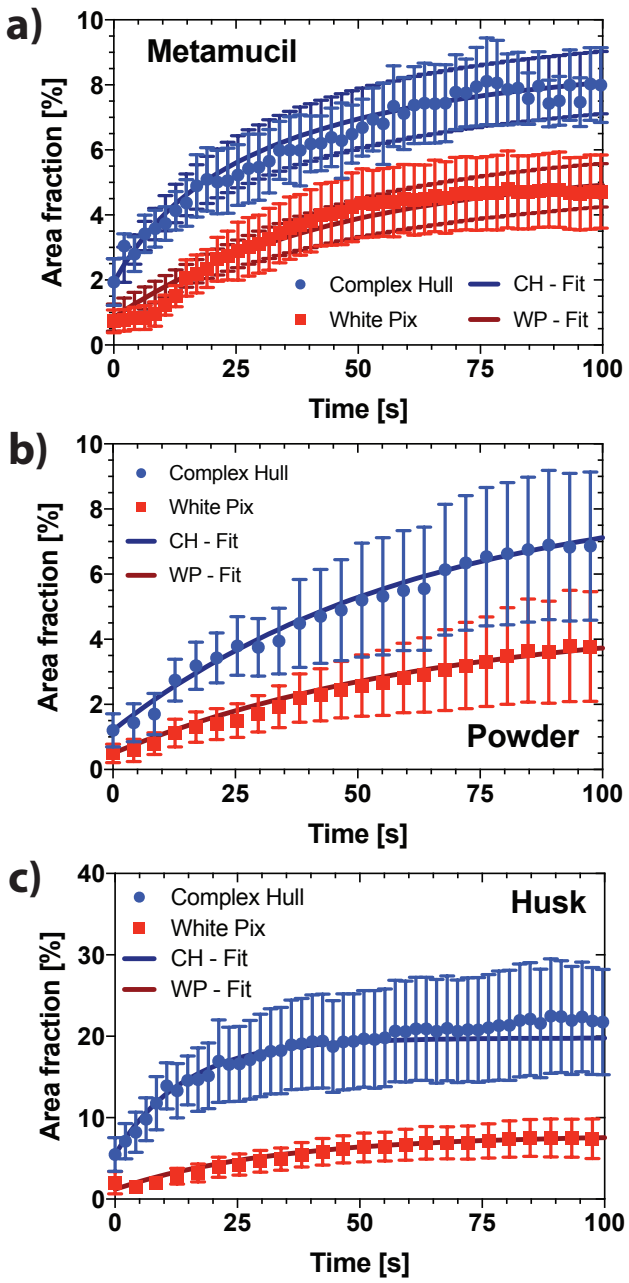

Figure 4S-4. Method comparison for single grain hydration for a) fine, b) medium, and c) coarse powder. Area fraction versus time was determined using two different image analysis techniques: the complex hull algorithm and the total number of white pixels from the binary images.

4.8 References

[1] J. R. Stokes, L. MacAkova, A. Chojnicka-Paszun, C. G. De Kruif, and H. H. J. De Jongh, Langmuir **27**, 3474 (2011).

[2] S. W. Cui, *Food Carbohydrates: Chemistry, Physical Properties and Applications* (2005).

[3] S. W. Cui and K. T. Roberts, *Dietary Fiber. Fulfilling the Promise of Added-Value Formulations* (2009).

[4] R. Lapasin, *Rheology of Industrial Polysaccharides: Theory and Applications* (Springer US, 1995).

[5] N. Gasbarro and M. J. Solomon, *Chitosan as a Yield Stress Fluid: Concentration Dependent Rheology and Microdynamics* (n.d.).

[6] L. M. Zhang and T. Kong, Colloid Polym. Sci. **285**, 145 (2006).

[7] C. Karakasyan, S. Lack, F. Brunel, P. Maingault, and D. Hourdet, Biomacromolecules **9**, 2419 (2008).

[8] J. Pourchez, A. Peschard, P. Grosseau, B. Guilhot, R. Guyonnet, and F. Vallée, ICPIC 04, 11th Int. Congr. Polym. Concr. (2004).

[9] S. Rossi, M. Marciello, G. Sandri, F. Ferrari, M. C. Bonferoni, A. Papetti, C. Caramella, C. Dacarro, and P. Grisoli, Pharm. Dev. Technol. **12**, 415 (2007).

[10] R. M. Savage, Food Hydrocoll. **14**, 209 (2000).

[11] A. R. Madgulkar, M. R. P. Rao, and D. Warrier, *Characterization of Psyllium (Plantago Ovata) and Its Uses* (Springer, Cham, 2015).

[12] L. Yu, G. E. Yakubov, W. Zeng, X. Xing, J. Stenson, V. Bulone, and J. R. Stokes, Carbohydr. Polym. **165**, 132 (2017).

[13] B. Singh, G. S. Chauhan, S. S. Bhatt, and K. Kumar, Carbohydr. Polym. **64**, 50 (2006).

[14] K. Evans and D. Burton, (2012).

[15] M. A. Hussain, G. Muhammad, I. Jantan, and S. N. A. Bukhari, Polym. Rev. **56**, 1 (2016).

[16] L. Yu and J. Perret, J. Agric. Food Chem. **51**, 492 (2003).

[17] M. Bhatia and M. Ahuja, Int. J. Biol. Macromol. **72**, 495 (2015).

[18] M. Mariotti, M. Lucisano, M. Ambrogina Pagani, and P. K. W. Ng, Food Res. Int. **42**, 963 (2009).

[19] M. R. Siahi-Shadbad, K. Asare-Addo, K. Azizian, D. Hassanzadeh, and A. Nokhodchi, AAPS PharmSciTech **12**, 1176 (2011).

[20] A. Farahnaky, H. Askari, M. Majzoobi, and G. Mesbahi, J. Food Eng. **100**, 294 (2010).

[21] J. Hughes and M. E. McCully, Stain Technol. **50**, 319 (1975).

[22] J. Schindelin, I. Arganda-Carreras, E. Frise, V. Kaynig, M. Longair, T. Pietzsch, S. Preibisch, C. Rueden, S. Saalfeld, B. Schmid, J.-Y. Tinevez, D. J. White, V. Hartenstein, K. Eliceiri, P. Tomancak, and A. Cardona, Nat. Methods **9**, 676 (2012).

[23] W. M. J. HUANG L K, Pattern Recognit. **28**, 41 (1995).

[24] S. van der Walt, J. L. Schönberger, J. Nunez-Iglesias, F. Boulogne, J. D. Warner, N. Yager, E. Gouillart, and T. Yu, PeerJ **2**, e453 (2014).

[25] R. Ahmadi, A. Kalbasi-Ashtari, and S. M. T. Gharibzahedi, Int. Agrophysics **26**, 91 (2012).

[26] J. J. Lietor-Santos, C. Kim, M. L. Lynch, A. Fernandez-Nieves, and D. A. Weitz, Langmuir **26**, 3174 (2010).

[27] M. M. Cross, J. Colloid Sci. **20**, 417 (1965).

Chapter 5 Conclusions and future directions

In this dissertation, we explored the connection between the microscopic dynamics and macroscopic rheology of two types of gels – fractal cluster colloidal gels with embedded active matter and psyllium polysaccharide gels.

In chapter 2, we characterized the microscopic dynamics of fractal cluster colloidal gels with embedded active colloids. We developed a model gel system to study the effects of active matter on colloidal gels by incorporating active Janus colloids into the fractal gel structure. We prepared gels by addition of a divalent salt, $MgCl_2$, to an initially stable suspension of polystyrene and platinum coated polystyrene Janus colloids, which incorporates the Janus colloids into the fractal gel. Hydrogen peroxide – the fuel that drives the diffusiophoretic motion of the embedded Janus colloids – is delivered to the gel by a porous hydrogel membrane. We characterized the dynamics of the gel network before and after addition of hydrogen peroxide. We found an increase in the dynamics of all particles in the gel network after addition of hydrogen peroxide. We characterized the amount of enhancement as a function of the total input of active energy – which is set by the hydrogen peroxide concentration and the ratio of active to passive particles. We modeled the dynamics of the gel network as a summation of the passive gel mobility, the direct motion of the active colloids, and the indirect contributions from a strain field induced on the passive gel by the active colloids.

We found significant changes in the dynamics of fractal cluster gels by embedding a small fraction of active colloids within the gel. Future work could analyze

how active motion affects other microdynamical changes such as the two-dimensional displacement field generated around an active colloid. In our experiments, we used an active colloid mechanism that utilizes platinum coated polystyrene Janus colloids and hydrogen peroxide to generate self-propulsion [1]. A by-product of this active colloid mechanism we used is oxygen [2]; at high enough concentrations, the oxygen cannot remain dissolved in the solution and will form disruptive gas bubbles. The formation of oxygen bubbles limited the amount of hydrogen peroxide that we could deliver to our gels. Future work could explore the incorporation of an active particle system that does not produce oxygen bubbles, such as particles activated by electric or magnetic fields [3], in order to explore the effects of high amounts of activity. With high enough activity, active motion could also induce changes in the gel microstructure, which could correspond to changes in the yield stress of the gel [4].

For our model of the gel dynamics, we used the strain field induced by the displacement of a particle embedded in a homogeneous elastic medium [5]. However, we found that our model slightly under-predicted the experimentally measured changes in the dynamics. Future work could further explore the application of the strain field for a homogeneous elastic medium to fractal cluster gels. We accounted for the fractal structure of the gel by multiplying the strain field by the radial distribution function of a fractal gel and integrate the product of the two to the average cluster size. Our model only accounted for intracluster effects of activity in colloidal gels. Future work to model the strain field of fractal gels could improve characterization of the dynamics of fractal gels with embedded active colloids.

In chapter 3, we characterize the effects of active matter on the rheology of fractal cluster colloidal gels. We compare the linear viscoelastic moduli of passive gels (comprised fully of Brownian polystyrene colloids) and active gels (comprised principally of Brownian polystyrene colloids with a small fraction of platinum coated polystyrene active colloids). We developed an experimental approach that incorporates oxygen permeable materials [6] into the rheometer tooling and anti-foam chemicals [7,8] to help suppress the formation of oxygen bubbles during measurements. We find the addition of active motion leads to a decrease in the viscoelastic moduli of fractal cluster colloidal gels. We observed decreases in the viscoelastic moduli by up to a factor of 8.5 for a small ratio of active to passive colloids ~ 10%.

We compared the frequency dependent viscoelastic moduli obtained from microrheology and mechanical rheology for passive and active gels. We found that microrheology is most accurate for passive gels at low frequencies and over-predicted the viscoelastic moduli of active gels across the full frequency range studied. We examined hypothesis that might explain the decrease in the modulus of the gel due to activity that were broadly divided into two categories: active motion induced changes to the gel structure and active motion acting on the gel structure to change the microdynamics.

Having found active matter leads to a decrease in the linear viscoelastic moduli of fractal gels, future studies could examine the effects of active motion on other rheological properties. We find a modest change in the onset of non-linearity for active gels with a low ratio of active to passive colloids and 5% hydrogen peroxide. With higher amounts of activity, the active motion could cause an even larger shift in the on-set of non-linearity. Active motion could also be used to aid in the recovery of gels after yielding.

Strain induced yielding leads to bond breakage of colloidal gels [4]; incorporating active motion could allow bonds to heal after they have undergone yielding.

In our experiments, the hydrogen peroxide that triggers active motion is added before initiation of gelation. After all of the hydrogen peroxide is consumed, and the active particles in the gel have resumed their Brownian motion, the modulus of the gel returns to values observed in the passive gels. Future studies could investigate the incorporation of a different active particle system to allow for better control of material properties. As an example, the active particle system used by Palacci et. al. can be turned off and on controllably with a blue light [9]. Incorporating a controllable active colloid system could allow for the creation of gels with re-configurable mechanical properties by turning on the active motion to have gels with a lower modulus and then turning off the activity to increase the modulus. Precise control over the rheological properties of gels through embedded active motion could be useful for industrial applications such as paints and coatings, pharmaceuticals, or agricultural formulations [5,10].

We also found that passive micorheology based on a generalized Stokes-Einstein equation over-predicted the frequency dependent viscoelastic moduli of active gels when compared to mechanical rheometry measurements. Application of the generalized Stokes-Einstein relation for microrheology requires validity of the fluctuation – dissipation theorem [11], which is not expected for active colloidal systems. Previous studies of active actin gels have shown a violation of the fluctuation – dissipation theorem in these gels [12]. Future work could address the extension of the fluctuation – dissipation theorem, and consequently a generalized Stokes-Einstein equation, to active colloidal suspensions.

In chapter 4, we characterize the kinetics of hydration and gelation for psyllium polysaccharide gels. Psyllium powders readily absorb water and swell to form a gel phase. However, under certain conditions, the gel undergoes syneresis and consolidates resulting in a dense gel phase underneath a polymer-poor aqueous phase. Our objective was to investigate the transition from powder to gel phase in order to understand why certain materials were more prone to syneresis. We characterized gels prepared with three different psyllium materials with varying powder size: fine, medium, and coarse. Steady state rheological measurements showed little difference in the steady state gels of the three materials as a function of concentration. However, transient rheological measurements showed significant differences between the three materials. We found that the gel that is more prone to syneresis (gels prepared with the fine powder) also demonstrated slower rheokinetics than the other two. This suggests a competition between sedimentation and gelation to generate a stable gel sample across all concentrations. The psyllium grains have a high density that could trigger consolidation and syneresis; gelation, or dynamic arrest, could trap the grains in a sample spanning network and suppress the effects of syneresis [13].

We further characterize the kinetics of hydration through microscopic measurements of the grains as they hydrate and expand. We deliver an aqueous solution containing fluorescent dye that binds with the psyllium grains and record videos of the grains during hydration. This approach allowed us to visualize the hydration process, which is stunning and dynamic. We quantified the rate of hydration by calculating the area fraction of the grains over time. From single grain studies, we observed an increase by up to a factor of eight in the grain size. We also characterized hydration times from

multi-grain interactions over a concentration range of 20 – 97%. We found the rate of hydration decreases with increasing concentration for the fine and medium powders; while the rate of hydration increases with the concentration of the coarse powder.

While transient rheology experiments showed variations between the three materials, the microscopic hydration measurements did not corroborate those differences. We found the single and multi-grain hydration times of the fine and medium powder were not statistically distinguishable. We do observe the timescales to reach a plateau value in the transient rheology experiments are comparable to the time scales observed in multi-grain hydration studies. Our findings suggest there are additional factors that govern the plateau viscosity and viscoelastic moduli; however the times to reach plateau values in transient rheology experiments are related to the kinetics of microscopic grain hydration. Future work could examine the differences in chemical interactions amongst the three psyllium materials, such as examining the functional groups present on the grain. Future studies could also examine the effects of polymer crystallinity or molecular weight distribution. In our experiments, we analyzed grains with three different sizes; probing a larger range of grain sizes could reveal information about the rheology and gel stability of psyllium gels.

5.1 References

[1] J. R. Howse, R. A. L. Jones, A. J. Ryan, T. Gough, R. Vafabakhsh, and R. Golestanian, Phys. Rev. Lett. **99**, 048102 (2007).

[2] M. A. Hasnat, M. M. Rahman, S. M. Borhanuddin, A. Siddiqua, N. M. Bahadur, and M. R. Karim, Catal. Commun. **12**, 286 (2010).

[3] C. W. Shields and O. D. Velev, Chem **3**, 539 (2017).

[4] L. C. Hsiao, R. S. Newman, S. C. Glotzer, and M. J. Solomon, Proc. Natl. Acad. Sci. **109**, 16029 (2012).

[5] M. H. Lee and E. M. Furst, Phys. Rev. E **77**, 041408 (2008).

[6] D. Dendukuri, D. C. Pregibon, J. Collins, T. A. Hatton, and P. S. Doyle, Nat. Mater. **5**, 365 (2006).

[7] A. J. O'Lenick, J. Surfactants Deterg. **3**, 229 (2000).

[8] Z. Németh, G. Rácz, and K. Koczo, J. Colloid Interface Sci. **207**, 386 (1998).

[9] J. Palacci, S. Sacanna, A. P. Steinberg, D. J. Pine, and P. M. Chaikin, Science. **339**, 936 (2013).

[10] R. M. Savage, Food Hydrocoll. **14**, 209 (2000).

[11] T. M. Squires and T. G. Mason, Annu. Rev. Fluid Mech. **42**, 413 (2010).

[12] D. Mizuno, C. Tardin, C. F. Schmidt, and F. C. MacKintosh, Science. **315**, 370 (2007).

[13] J. J. Lietor-Santos, C. Kim, M. L. Lynch, A. Fernandez-Nieves, and D. A. Weitz, Langmuir **26**, 3174 (2010).

Appendix A: Active gel theory

Active colloids embedded in a fractal cluster gel increase the average mean squared displacement of particles in the gel. Here, a theory for the enhanced average displacement is described. The radial distribution function of a fractal cluster gel for r >4a is:

$$g(r) = \frac{c}{a^{D_F}} r^{D_F - 3} \exp\left(-\left(\frac{r}{R_c}\right)^{\gamma}\right) \quad (1)$$

where a is the particle radius, D_F is the fractal dimension, R_c is the cluster radius, c is a prefactor, and γ is the cutoff exponent [1]. For r < 4a, we use the experimentally measured g(r), because pair structure on this scale can be sensitive to details of the aggregation mechanism. The mean squared localization of a Brownian particle in a fractal cluster gel is, from Krall and Weitz [2]:

$$\lim_{t \to \infty} < x^2(t) > = \frac{k_B T}{\pi R_c G} \quad (2)$$

Here k_bT is the thermal energy and G is the elastic modulus of the gel. We hypothesize that the localization of an active particle in such a gel is enhanced by a factor of:

$$\frac{<U^2>}{<x^2(t)_{passive}>} = \frac{E_{active}}{E_{passive}} = \frac{6\pi\mu a V l}{k_B T} \quad (3)$$

Here $<U^2>$ is the mean squared displacement of an active particle in the gel; this notation is chosen consistent with the strain field discussion that follows. V is the velocity of a free, active particle in a fluid of viscosity μ, and l is the active particle run length given by $l = \tau_R V$, where τ_R is the reorientation time. This expression is consistent with active colloids exerting a swim pressure characterized by run speed and length [3]. As

described in the main text, eqn (3) is consistent with direct measurement of the enhanced localized dynamics of the active Janus particles in the otherwise passive gel.

The active particle deformation induces a strain field in the region that surrounds it. Because we develop a dilute theory, without loss of generality we can take the active particle displacement as in the x-direction. Then, for this active particle deformation **U** = $U_x\mathbf{e_x}$ and the (anisotropic) induced strain field is:

$$\mathbf{u}(\mathbf{x}) = \frac{3a}{10-12v}\left[\left(\frac{3-4v}{r}+\frac{a^2}{3r^3}\right)\mathbf{U}+\left(1-\frac{a^2}{r^2}\right)\frac{\mathbf{U}\cdot\mathbf{xx}}{r^3}\right] \tag{4}$$

where v is the Poisson ratio and boldface type indicated vectors [4] . The components of the strain field are given by:

$$u_x(r,\theta,\phi) = \frac{3a}{10-12v}\left[\left(\frac{3-4v}{r}+\frac{a^2}{3r^3}\right)U_x+\left(1-\frac{a^2}{r^2}\right)\frac{U_x(r\sin\theta\cos\phi)^2}{r^3}\right] \tag{5}$$

$$u_y(r,\theta,\phi) = \frac{3a}{10-12v}\left[\left(1-\frac{a^2}{r^2}\right)\frac{U_x}{r^3}\,r^2\sin^2\theta\sin\phi\cos\phi\right] \tag{6}$$

$$u_z(r,\theta,\phi) = \frac{3a}{10-12v}\left[\left(1-\frac{a^2}{r^2}\right)\frac{U_x}{r^3}\,r^2\sin\theta\cos\phi\cos\theta\right] \tag{7}$$

where θ is the polar and ϕ is the azimuthal angle. Rearrangement of equation 3 yields the active particle mean squared displacement, $<U^2>$:

$$< U^2 >= \frac{E_{Active}}{k_BT}\langle x^2(t)\rangle_{passive\ gel} \tag{8}$$

where brackets denote time averaged quantities. The mean squared induced displacement due to the active particle is computed from the results of eqn (5) – (7):

$$< u(r,\theta,\phi)^2 >=< u(r,\theta,\phi)_x^2 > +< u(r,\theta,\phi)_y^2 > +< u(r,\theta,\phi)_z^2 > \tag{9}$$

The active particle generates a strain field that extends over the full cluster volume. The mean-squared displacement enhancement of the active gel is:

$$\delta(t) = 1 + X_{active}\left\{\frac{E_{active}}{k_B T}\right.$$

$$\left. + X_{passive}\int_{2a}^{R_c} 4\pi r^2 dr \int_0^{\pi} \sin\,\theta d\theta \int_0^{2\pi} g(r) < u(r,\theta,\phi)^2 > d\phi \right\} \quad (10)$$

The notation indicates that the anisotropic strain field is integrated over all positions within the cluster. As in the main text, X_{active} and $X_{passive}$ are the mole fraction of each type of colloid in the gel. In equation 10, the first term is due to Brownian motion. The second term includes a direct contribution of the active particle and an indirect contribution from the induced, anisotropic strain-field, weighted by the probability of finding a passive particle a distance (r) in the fractal cluster from the active particle. Using equation 10, the direct and indirect contributions are:

$$\delta_{direct} = X_{active}\frac{E_{active}}{k_B T} \quad (11)$$

$$\delta_{indirect} = X_{passive}\int_{2a}^{R_c} 4\pi r^2 dr \int_0^{\pi} \sin\,\theta d\theta \int_0^{2\pi} g(r) < u(r,\theta,\phi)^2 > d\phi \quad (12)$$

Equation 10 contains no fitting parameters; all of the values are determined from experimental measurements or the simulations of Lattuada et. al. [1]. The value of E_{active} used in equation 10 is calculated for each hydrogen peroxide concentration using equation 3. We use the experimentally measured g(r) for 2a < r < 4a and eqn (1) for r > 4a, where values of c and R_c are determined from fits to the experimental data and the passive gel volume fraction of 0.005, the fractal dimension, D_F, is 1.8, as determined from Figure 1e, and the cutoff exponent, γ, is 2.3, as in ref [1].

We find that the model is relatively insensitive to the Poisson ratio used from ν = 0.25 – 0.5, which is a common range for soft materials [5]. The predicted enhancement, δ, in this range of Poisson ratios changes by less than 0.1%, shown in Table A-2. The

upper limit of integration in equation 10 is set at the cluster radius, R_c; however, the model predictions are relatively insensitive to the upper integration limit provided that it is at least as large as the cluster radius. For example, if the upper integration limit is varied from Rc to 10*Rc, the change in the predicted enhancement, δ, is less than 2%, shown in Table A-2.

% H_2O_2 Delivered	% H_2O_2 in gel sample	% PtPS	V	l	E_a/E_b	X_aE_a/X_bE_b
3	2	0.05	1.13	3.9	4.5	2.3
5	3.3	0.05	1.19	4.1	5.0	2.5
8	5.3	0.05	1.35	4.6	6.5	3.2
10	6.7	0.05	1.58	5.4	8.9	4.4
12	8	0.05	1.63	5.6	9.4	4.7
5	3.3	0.065	1.19	4.1	5.0	3.3
5	3.3	0.12	1.19	4.1	5.0	6.0
5	3.3	0	0	0	0	0
1.5	1	0.05	0.5	1.7	0.9	0.4

Table A-1 Active particle velocity (V) and run length (l), ratio of active to passive energies (E_a/E_b), and X_aE_a/X_bE_b at each hydrogen peroxide concentration and ratio of active to passive particles. Velocity is shown in units μm/s and run length is in μm.

Poisson Ratio	Delta
0.26	1.444
0.3	1.444
0.34	1.444
0.38	1.444
0.42	1.445
0.46	1.445
0.5	1.446

Upper limit of integration	Delta
25	1.437
50	1.441
100	1.446
250	1.455

Table A-2. Determining the sensitivity of predicted enhancement to left) Poisson ratio used in strain field and right) upper limit of integration.

a

Height (μm)	# PS	# PtPS	% PtPS
0-2	80 ± 20	46 ± 6	60 ± 7
0-4	150 ± 30	61 ± 7	41 ± 7
0-6	220 ± 40	63 ± 8	29 ± 4
0-8	270 ± 40	63 ± 8	23 ± 4
0-10	330 ± 50	63 ± 8	19 ± 4
0-15	460 ± 100	63 ± 8	14 ± 4
0-20	500 ± 60	63 ± 8	13 ± 3

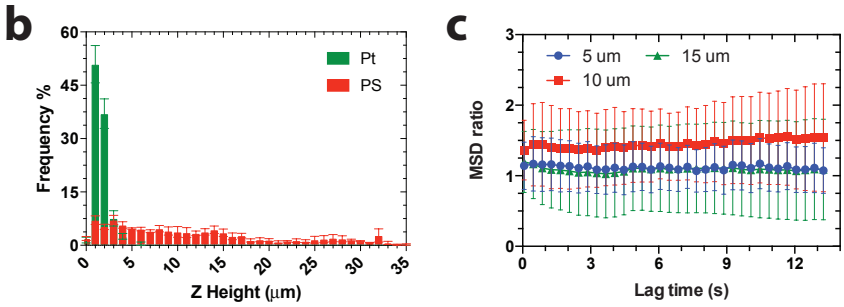

Figure A-1. 3D distribution of Janus colloids in gel. A) Cumulative number of polystyrene and Janus particles measured in an active gel by 3D CLSM, B) Probability distribution of polystyrene and Janus particles as a function of distance above the coverslip, and C) mean squared displacement enhancement (error bars are standard deviation) as a function of z height for an active gel with1:8 ratio of active passive particles and 6.7% H_2O_2. The Janus particle concentration is highest closest to the coverslip and decreases further into the sample, whereas the concentration of polystyrene particles is more uniformly distributed. The mean squared displacement at 5, 10, and 15 microns above the coverslip are however not distinguishable.

References

[1] M. Lattuada, H. Wu, and M. Morbidelli, J. Colloid Interface Sci. **268**, 106 (2003).

[2] A. H. Krall and D. A. Weitz, Phys. Rev. Lett. **80**, 778 (1998).

[3] S. C. Takatori, W. Yan, and J. F. Brady, Phys. Rev. Lett. **113**, 28103 (2014).

[4] M. H. Lee and E. M. Furst, Phys. Rev. E **77**, 41408 (2008).

[5] R. H. Pritchard, P. Lava, D. Debruyne, and E. M. Terentjev, Soft Matter **9**, 6037 (2013).

Appendix B: Reaction kinetics of H_2O_2 decomposition

Platinum catalyzes the decomposition of hydrogen peroxide (H_2O_2) into water and oxygen via the following chemical reaction [1]:

$$2H_2O_2 \rightarrow 2\,H_2O + O_2$$

For our experiments, we add 100 μL of hydrogen peroxide at various concentrations given by C_1 to a gel with a final volume of 2mL. To determine the final concentration of H_2O_2, we use the expression: $C_1V_1 = C_2V_2$. The added and final concentration for our experiments is shown in Table 1.

% H_2O_2 Added	Final Conc [%]	mMol H_2O_2	mol/L H_2O_2
2.5	0.125	0.07	0.035
5	0.25	0.15	0.075
7.5	0.375	0.22	0.11
10	0.5	0.29	0.145

Table B-1. Initial concentration of hydrogen peroxide.

Concentrations in Table 1 are given in units of %w/v. The rate constant for the decomposition of H_2O_2, k, is given by:

$$k = \frac{k_2[H_2O_2]}{[H_2O_2] + k_2/k_1}$$

where $k_1 = 4.4 \times 10^{11}$ μm^{-2} s^{-1} and $k_2 = 4.8 \times 10^{10}$ μm^{-2} s^{-1} [2]. The overall rate of reaction, r, is given by:

$$r = -k[H_2O_2]$$

Because k has units of s^{-1} μm^{-2}, we need to multiply k by the available surface area of Platinum so that k has units consistent with first order reaction kinetics. To calculate the amount of Platinum, consider the surface area of a sphere:

$$A = 4\pi r^2$$

where r is the radius of the platinum coated sphere. Because our particles have a diameter of 1 μm and we add a coating of 10 nm Platinum, the final radius of the particle is r = 0.5 μm + 10 nm. The total amount of Platinum is then $N_{PtPS}\left(\frac{A}{2}\right)$, where N_{PtPS} is the total number of Janus particles. The rate of reaction then becomes:

$$r = -k\left(\frac{A}{2}\right)N_{PtPS}[H_2O_2]$$

To solve for the amount of H_2O_2 versus time:

$$r_{H2O2} = -k[H_2O_2] = \frac{1}{V}\frac{dN_{H2O2}}{dt}$$

where N_{H2O2} is moles of H_2O_2 and V is the volume, which is 2mL for our experiments. Since volume is constant during the experiments, we can write the rate expression in terms of the concentration of H_2O_2, C_{H2O2}.

$$-k[H_2O_2] = \frac{1}{V}\frac{d(C_{H2O2}V)}{dt}$$

$$-k[H_2O_2] = \frac{dC_{H2O2}}{dt}$$

We can use two approaches to solve for C_{H2O2}. In the simple approach, we treat k as a constant independent of $[H_2O_2]$. In this approach the rate expression is:

$$\frac{dC_{H2O2}}{dt} = -k[H_2O_2]$$

We can solve directly for the concentration of hydrogen peroxide, resulting in:

$$\ln[H_2O_2] = -kt + C$$

Our initial condition to solve for C is t = 0, $[H_2O_2] = C_0$. Plugging in and solving for C, gives:

$$\ln H_2O_2 = -kt + \ln C_O$$

Rearranging the equation above:

$$[H_2O_2] = C_0 \exp(-kT)$$

Using this approach, we find that the H_2O_2 consumption happens on timescales $t \sim 10^6$.

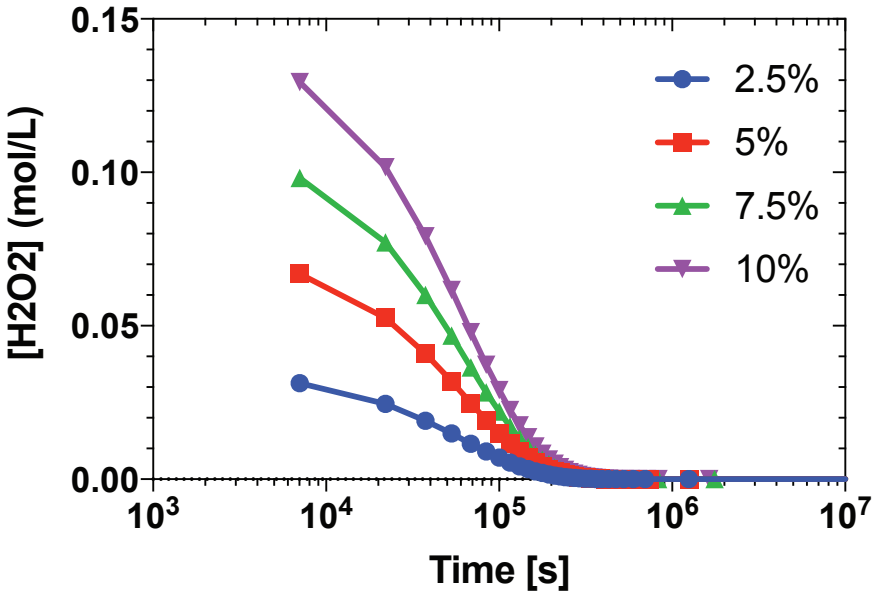

Figure B-1. Hydrogen peroxide concentration as a function of time estimated from H_2O_2 independent reaction constant.

We can also apply a more rigorous approach using the expression for k as a function of $[H_2O_2]$. In this approach, C_{H2O2} is given by:

$$\frac{dC_{H2O2}}{dt} = -\frac{k_2[H_2O_2]}{[H_2O_2] + \frac{k_2}{k_1}}[H_2O_2]$$

$$\frac{dC_{H2O2}}{dt} = -\frac{k_2[H_2O_2]^2}{[H_2O_2] + \frac{k_2}{k_1}}$$

This functional form of the differential equation cannot be solved easily by hand, so we use a numerical integration method to solve for C_{H2O2}. This method results in timescales that are ~ 10^9 sec.

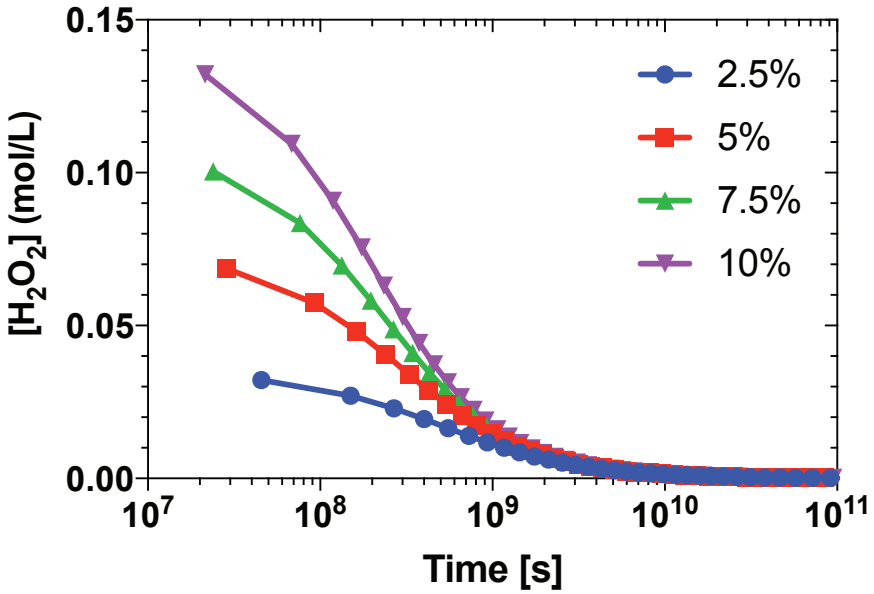

Figure B-2. Hydrogen peroxide concentration as a function of time modeled using rate equation for H_2O_2 decomposition from Howse et. al. [2].

References

[1] T. A. Vetter and D. P. Colombo, J. Chem. Educ. **80**, 788 (2003).

[2] J. R. Howse, R. A. L. Jones, A. J. Ryan, T. Gough, R. Vafabakhsh, and R. Golestanian, Phys. Rev. Lett. **99**, 048102 (2007).